Chapter – 3

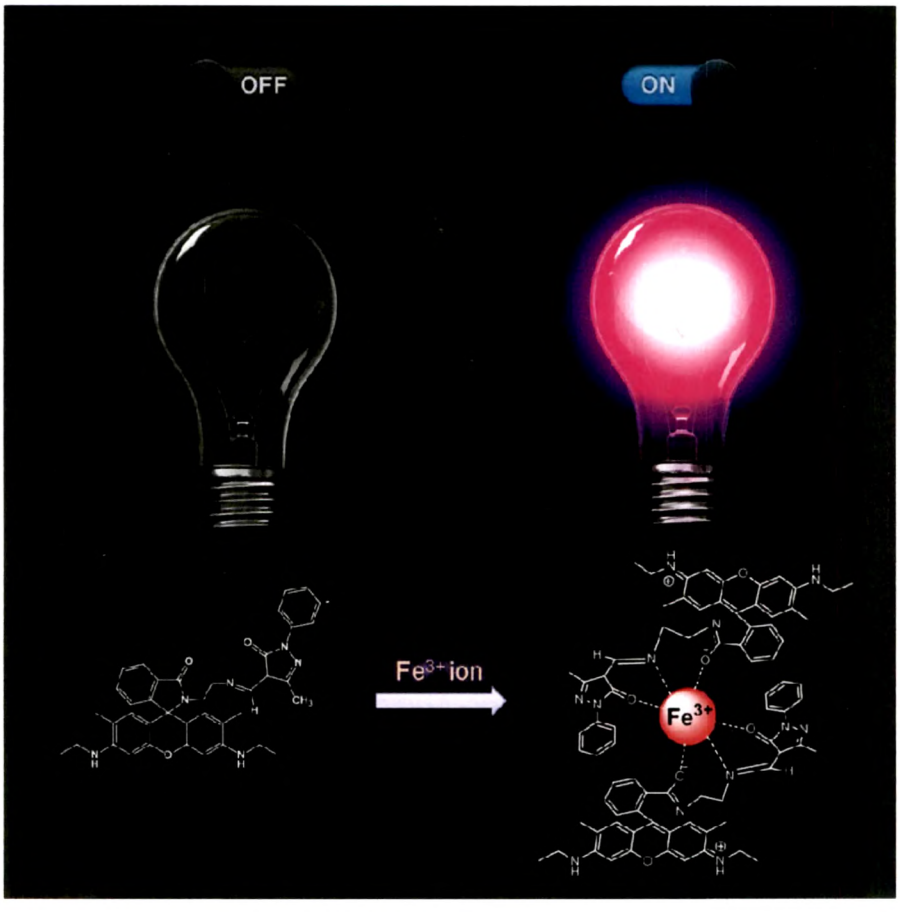

Design, synthesis and characterization of rhodamine-pyrazolone based fluorescent molecular sensors

3.1. Introduction

The recognition and sensing of biologically and environmentally important species is of great interest to many scientists, including chemists, biologists, clinical biochemists and environmentalists in recent years [1-8]. Numerous analytical methods that are available for the detection of target concerned such that flame photometry, atomic absorption spectrometry, high-performance liquid chromatography, mass spectrometry, ion sensitive electrodes, electron microprobe analysis, neutron activation analysis, etc. have been developed [9-11]. However, these methods are expensive and time consuming procedures that involves sophisticated instrumentation and do not allow continuous monitoring. Fluorogenic methods in conjunction with suitable probes offer distinct advantages for the measurement of these analytes because fluorimetry is rapidly performed, is nondestructive, is highly sensitive and selective, is suitable for high-throughput screening applications, and can afford real information on the localization and quantity of targets of interest [2, 6-8, 13-15]. Therefore, considerable efforts are being made to develop selective fluorescent sensors for the detection of targeted species. To date various fluorescent molecular sensors with different excitation and emission wavelengths have been employed such as coumarin, pyrene, 1,8-naphthalamide, xanthenes, squaraine, cynine, boron dipyrromethene difluoride (BODIPY), nitrobenzofurazan, etc [1-8, 16, 17].

3.1.1. Phenomena of fluorescence

Luminescence is an emission of ultraviolet, visible or infrared photons from an electronically excited species. The word luminescence, which comes from the Latin (*lumen* = light) was first introduced as *luminescenz* by the physicist and science historian Eilhardt Wiedemann in 1888,to describe 'all those phenomena of light which are not solely conditioned by the rise in temperature', as opposed to incandescence. Luminescence is *cold light* whereas incandescence is *hot light* [18].

Fluorescence and phosphorescence are the type of luminescence. The term *phosphorescence* comes from the Greek word *phosphor* means 'which bears light'. The term phosphor has indeed been assigned since the middle Ages to materials that glow in the dark after exposure to light. The term fluorescence was introduced by Sir George Gabriel Stokes, a physicist and professor of mathematics at Cambridge in the

middle of the nineteenth century. The Jablonski diagram is convenient for visualizing in a simple way to understand the process of fluorescence and phosphorescence.

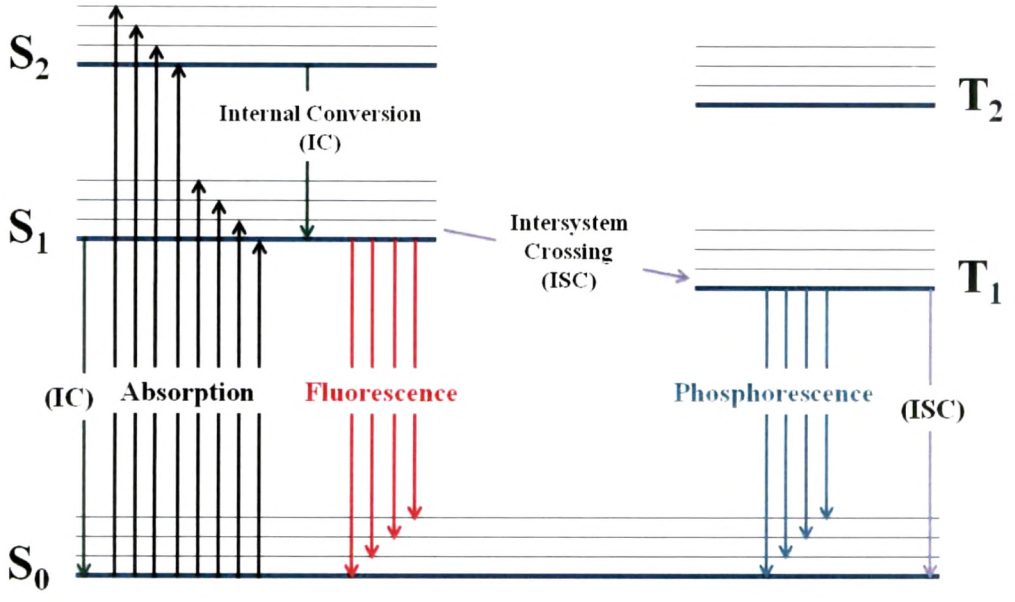

Figure 3.1. Jablonski diagram.

A typical Jablonski diagram is shown in Figure 3.1. The singlet ground, first, and second electronic states are represented by S_0, S_1, and S_2, respectively. The transitions between states are depicted as vertical lines to illustrate the instantaneous nature of light absorption. Absorption of a photon can bring a molecule to one of the vibrational levels of S_0, S_1, S_2 ... The transitions occur in about 10^{-15} s, a time too short for significant displacement of nuclei. The subsequent possible de-excitation processes are as follows:

Internal conversion (IC)

Internal conversion is a non-radiative transition between two electronic states of the same spin multiplicity. In solution, this process is followed by a vibrational relaxation towards the lowest vibrational level of the final electronic state. The excess vibrational energy can be indeed transferred to the solvent during collisions of the excited molecule with the surrounding solvent molecules. When a molecule is excited to an energy level higher than the lowest vibrational level of the first electronic state, vibrational relaxation (and internal conversion if the singlet excited state is higher

than S_1) leads the excited molecule towards the 0 vibrational level of the S_1 singlet state with a time scale of 10^{-13}-10^{-11} s.

From S_1, internal conversion to S_0 is possible but it is less efficient than the conversion from S_2 to S_1, because of the much larger energy gap between S_1 and S_0. Therefore, internal conversion from S_0 to S_1 occurs with emission of photons (fluorescence) and intersystem crossing to T_1 from which emission of photons (phosphorescence) can be observed.

Fluorescence

Emission of photons accompanying the $S_1 \rightarrow S_0$ relaxation is called *fluorescence*. Fluorescence is emission of light from singlet excited states, in which the electron in the excited orbital is paired (by opposite spin) to the second electron in the ground-state orbital. The emission rates of fluorescence are typically 10^8 s^{-1}, so that a typical fluorescence life time is near 10 ns (10×10^{-9} s). Because of the short timescale of fluorescence, measurement of the time-resolved emission requires sophisticated optics and electronics. According to the Stokes Rule, the wavelength of a fluorescence emission should always be higher than that of absorption [18].

The differences between the vibrational levels are similar in the ground and excited states, so that the fluorescence spectrum often resembles the first absorption band ('mirror image' rule). The gap (expressed in wavenumbers) between the maximum of the first absorption band and the maximum of fluorescence is called the Stokes shift.

Intersystem crossing

Intersystem crossing is a non-radiative transition between two isoenergetic vibrational levels belonging to electronic states of different multiplicities. For example, an excited molecule in the 0 vibrational level of the S_1 state can move to the isoenergetic vibrational level of the T_n triplet state; then vibrational relaxation brings it into the lowest vibrational level of T_1. Intersystem crossing may be fast enough (10^{-7}-10^{-9} s) to compete with other pathways of de-excitation from S_1 (fluorescence and internal conversion $S_1 \rightarrow S_0$). The probability of intersystem crossing depends on the singlet and triplet states involved. If the transition $S_0 \rightarrow S_1$ is of $n \rightarrow \pi^*$ type for instance, intersystem crossing is often efficient.

Phosphorescence

In solution at room temperature, non-radiative de-excitation from the triplet state T_1, is predominant over radiative de-excitation called *phosphorescence*. Phosphorescence is emission of light from triplet excited states, in which the electron in the excited orbital has the same spin orientation as the ground-state electron. Transitions to the ground state are forbidden and the emission rates are slow, so that phosphorescence lifetimes are typically milliseconds to seconds (10^3 to 10^0 s^{-1}). Even longer lifetimes are also possible. Following exposure to light, the phosphorescence substances glow for several minutes while the excited phosphors slowly return to the ground state. The phosphorescence spectrum is located at wavelengths higher than the fluorescence spectrum because the energy of the lowest vibrational level of the triplet state T_1 is lower than that of the singlet state S_1.

The recognition and detection of the desired analytes using chromogenic/ fluorogenic host molecules, which show selectivity towards a specific analyte, have gained significant interest in the last decades in the field of host-guest chemistry. These colorimetric and fluorogenic receptor molecules allow the detection of the targeted analyte through binding induced changes in the optical response in the form of electronic and fluorescence spectral changes.

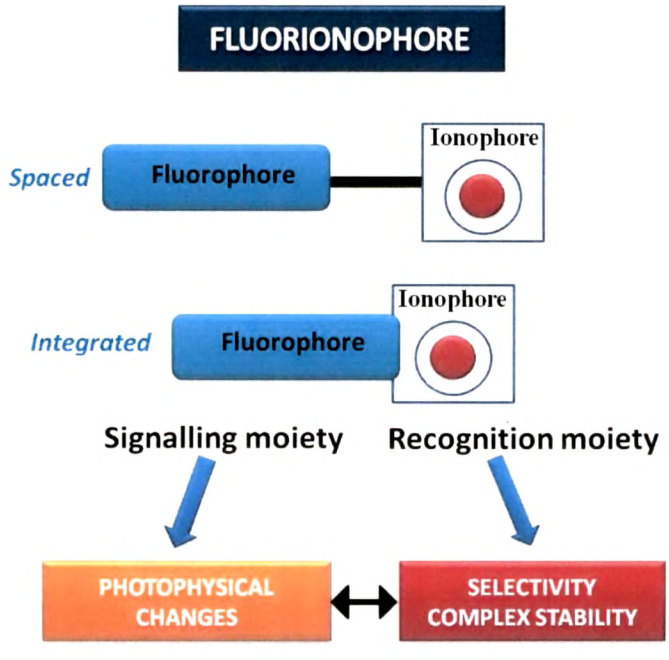

Figure 3.2. Main aspects of fluorescent molecular sensors for cation recognition.

3.1.2. Design of fluorescent molecular sensor

Fluorescent sensors consists of a fluorophore (fluorescent molecule) covalently linked to an ionophore (e.g. crown ether) and is thus called a fluoroionophore which selectively bind alkali, alkaline and transition metal ions. The ionophore is required for selective binding of the substrate, while the fluorophore provides the means of signalling this binding, whether by fluorescence enhancement or inhibition.

The *signalling moiety* acts as a signal transducer, i.e. it converts the information (recognition event) into an optical signal expressed as the changes in the photophysical characteristics of the fluorophore (*see* Figure 3.2). These changes are due to the perturbation (by the bound cation) of photoinduced processes such as electron transfer, charge transfer, energy transfer, excimer or exciplex formation or disappearance, etc.

3.1.3. Photophysical mechanisms of fluorescent sensors

3.1.3.1. Photoinduced electron transfer (PET)

Photoinduced electron transfer (PET) is the most widely used mechanistic pathway, which has been employed for designing receptors for cationic analytes. The working principle of a PET-based sensor is summarized in Figure 3.3.

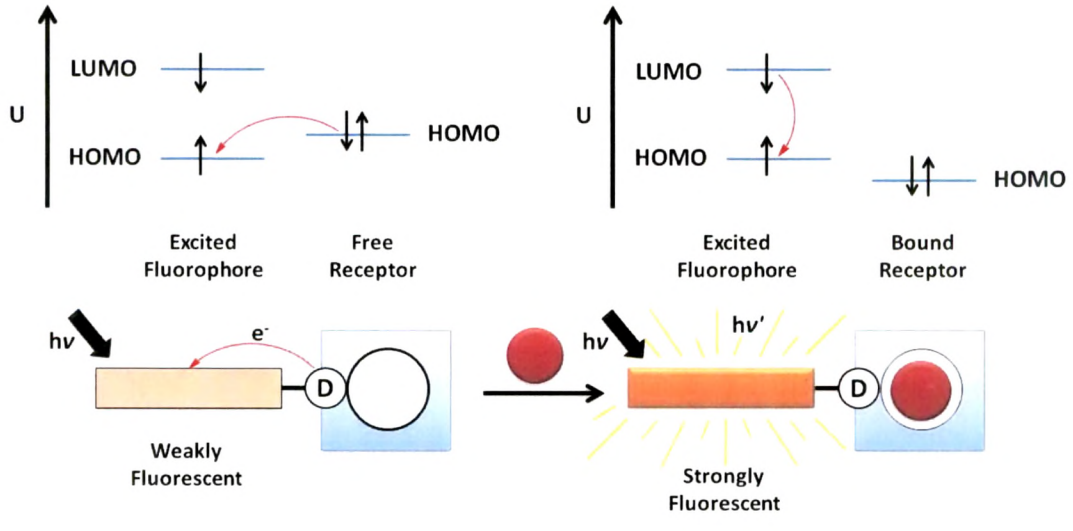

Figure 3.3. Principle of cation recognition by fluorescent PET sensors [14].

The designing principle for the PET based sensors involve a fluorophore connected with a receptor unit via a spacer. Excitation of the fluorophore promoted an electron of highest occupied molecular orbital (HOMO) to the lowest unoccupied molecular orbital (LUMO). The energetically feasible electron transfer enables PET and quenches the fluorescence of the fluorophore and thus fluorescence is absent at this stage. When cation binds with the receptor unit, the redox potential of the donor is raised so that the relevant HOMO becomes lower in energy and electron transfer is no longer energetically feasible consequently, PET is not possible anymore and fluorescence quenching is suppressed. Therefore, the capture of electron transfer after cation binding allows all the excited state electrons come back to the ground state and make the fluorophore highly fluorescent.

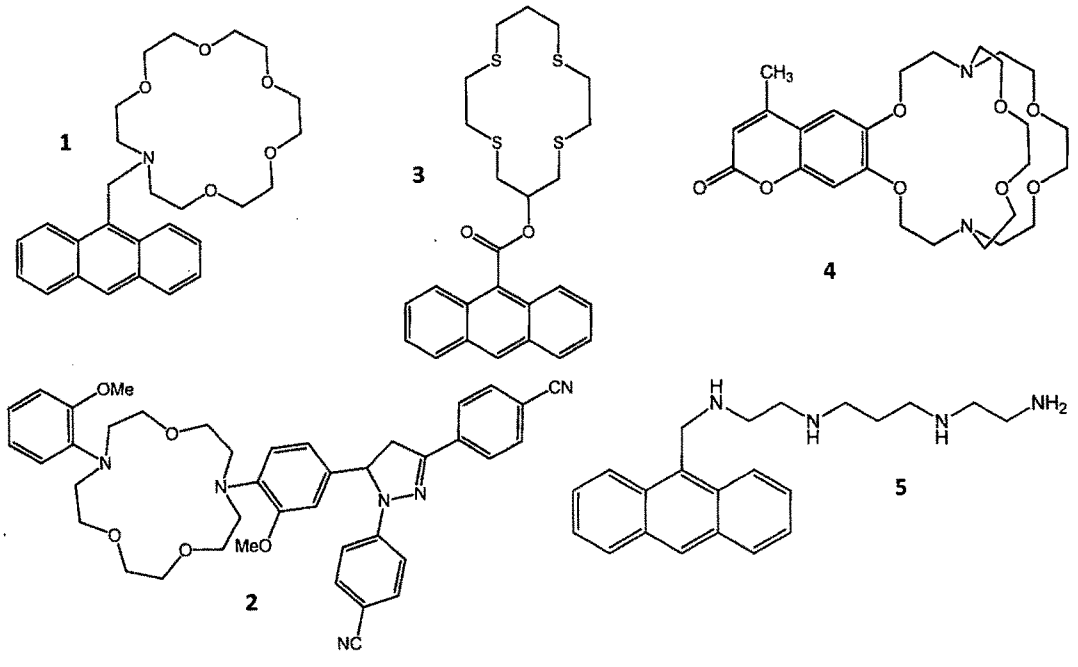

Figure 3.4. Structures of PET based fluorescent sensors.

Selected examples of PET based fluorescent sensors are depicted in Figure 3.4. The first and simplest coronand PET sensor **1** was reported by de Silva et al [19]. Upon binding with K^+ in methanol fluorescence quantum yield of PET sensor 1 increase from 0.003 to 0.14. In the sensor **2** [20] the methoxy groups are in ortho position to the nitrogen atoms of the crown participate in the complexation to achieve strong binding with Na^+ and accompanied with switching 'on' the fluorescence. The crown in the sensor **3** contains sulfur atoms, which are known for strong affinity

towards Cu^{2+}. This sensor is also based on PET principle and quenching of fluorescence occurs upon Cu^{2+} binding [21]. Sensor **4** is the example of macrobicyclic structure and it is expected to be more selective to alkali cations in compare to macrocyclic structures. The cavity of **4** fits well with the size of K^{+} and it has been successfully used for monitoring potassium level in blood and across biological membrane [22]. The podand-based sensor **5** [23]contain polyamine chain and used for the binding of Zn^{2+}, however it also shows strong binding with Cu^{2+}.

3.1.3.2. Energy transfer quenching (ET)

Most of the PET fluorescent sensors are designed on the basis of mechanism shown in Figure 3.5, however in some cases; other PET-based processes can also be possible upon complexation of transition metal ions. A transition metal ion can quench an excited fluorophore via an electron transfer mechanism, either by a bimolecular or an intramolecular process, if it possesses empty or half-filled d orbitals of appropriate energy. The transition metals exhibit redox activity and electron transfer can occur from the fluorophore to the bound metal ion, or vice versa, which results in quenching of the fluorophore by non-radiative energy transfer according to the Dexter mechanism in which a metal ion can quench the fluorescence of the excited state of the fluorophore by an energy transfer mechanism [4, 24].

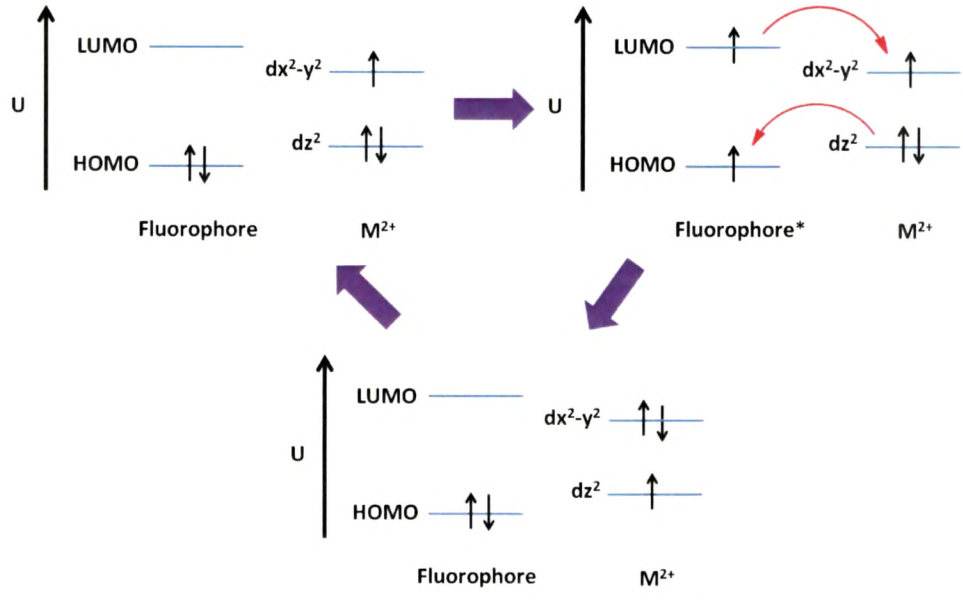

Figure 3.5. Mechanism for electron transfer (ET) in system containing an excited fluorophore and a d^0 metal ion.

Bergonzi et al. reported that the system shown in Figure 3.6 represents an example of molecular switch of fluorescence, whose OFF situation is generated by an ET process involving the fluorophore and the Cu^{II} centre [25]. The CuII ion is capable of quenching the fluorescence of naphthalene ring by electron transfer (ET) mechanism. The metal ion quenches the fluorescence through double electron exchange without affecting the net distribution of electron.

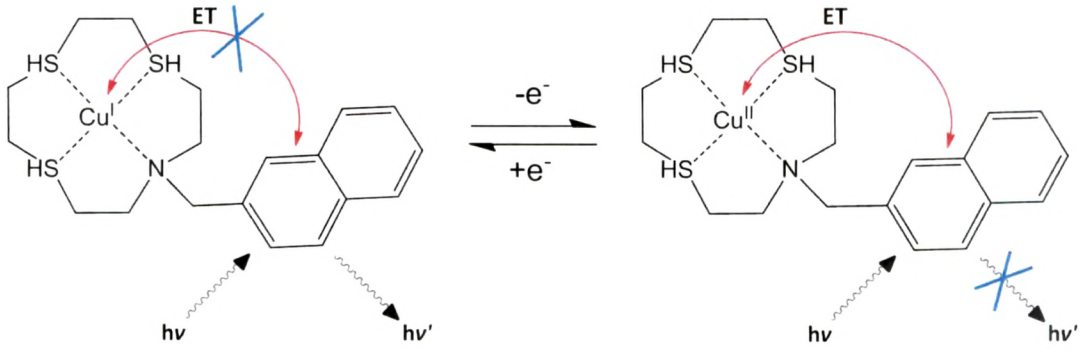

Figure 3.6. Double electron exchange between excited fluorophore and d^9 metal ion. The Cu^{II} centre promotes an ET process causing fluorescence quenching.

3.1.3.3. Resonance Energy Transfer

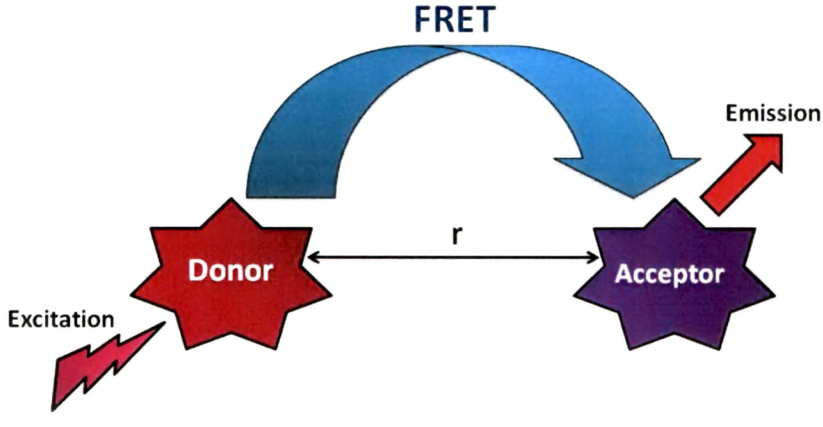

Figure 3.7. Schematic presentation of FRET process.

The mechanism of fluorescence resonance energy transfer (FRET) was first elucidated by T. Förster and also called Förster resonance energy transfer. FRET is a non-radiative transfer of energy from an excited state donor **D** to a proximal ground

state acceptor **A** through long-range dipole–dipole interactions. FRET is influenced by three factors: the distance between the donor and the acceptor, the extent of spectral overlap between the donor emission and acceptor absorption spectrum and the relative orientation of the donor emission dipole moment and acceptor absorption moment. FRET usually occurs over distances comparable to the dimensions of most biological macromolecules, that is, about 10 to 100 Å [15, 26].

Upon excitation, the excited state donor molecule transfers energy nonradiatively to a proximal acceptor molecule located at the distance *r* from the donor (*see* Figure 3.7). The acceptor releases the energy either through fluorescence or nonradiative channels [27].

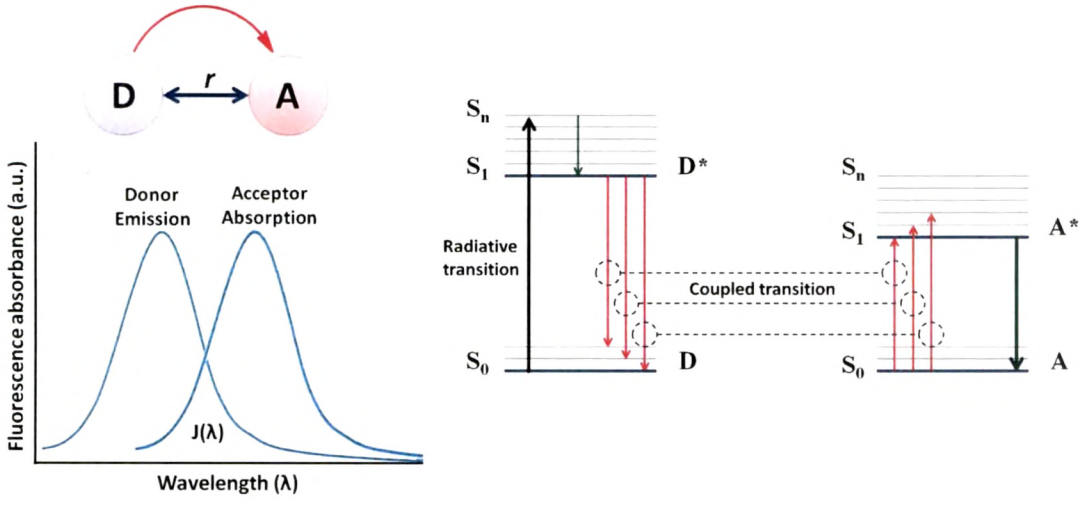

Figure 3.8. (A) Spectral overlap between donor based emission and acceptor based absorption bands and (B) Fluorescence (Förster) resonance energy transfer system.

The energy-transfer mechanism can be described as follows [28]:

$D + hv_0 \rightarrow D^*$	absorption
$D^* \rightarrow D + hv_1$	fluorescence
$D^* \rightarrow D$	nonradiative de-excitation
$D^* + A \rightarrow D + A^*$	energy transfer
$A^* \rightarrow A$	nonradiative de-excitation
$A^* \rightarrow A + hv_2$	induced fluorescence

The rate of energy transfer depends upon the extent of spectral overlap of the emission spectrum of the donor and the absorption spectrum of the acceptor, the quantum yield of the donor and the relative orientation of the donor and acceptor dipoles and the distance between the donor and acceptor units (*see* Figure 3.8). FRET is particularly wildly used to determine distances in biomolecules and supramolecular associations and assemblies. In the area of modern analytical research FRET as an operating principal has been extensively used by several researchers for metal ion recognition studies. Das *et al* reported a FRET based *off-on* fluorescent sensor **6** for Hg^{2+} ions [29]. Li *et al* developed a FRET-based sensor **7** for imaging Cr^{3+} in living cells [30] (*see* Figure 3.9).

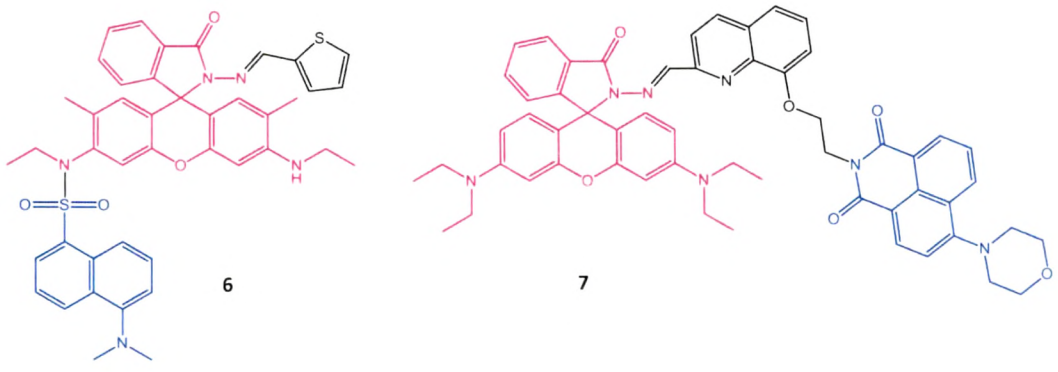

Figure 3.9. FRET-based fluorescent sensors.

3.1.3.4. Photoinduced Charge Transfer (PCT)

A fluorophore having an electron-donating group, conjugated to an electron-withdrawing group, favours a photoinduced intramolecular charge transfer (PCT) from the donor to the acceptor upon excitation with radiation of appropriate wavelength. The consequent change in dipole moment results in a Stokes shift that depends on the microenvironment of the fluorophore. Thus, the cations interaction with the donor or the acceptor moiety changes the photophysical properties of the fluorophore because the complexed cation affects the efficiency of intramolecular charge transfer [31-33].

Interaction of the donor fragment with the cation reduces the electron-donating character of this group, which disfavour the PCT process and thus a blue shift of the absorption spectrum is expected together with a decrease of the extinction coefficient. On the contrary, interaction of the cation with the acceptor group is expected to

favour the electron-withdrawing character and consequently the PCT process along with the increase in dipole moment. All these are expected to contribute to the red-shift of the absorption spectra with higher molar absorption coefficient value. The fluorescence spectra for such cases are expected to shift to the same direction as those of the absorption spectra (*see* Figure 3.10).

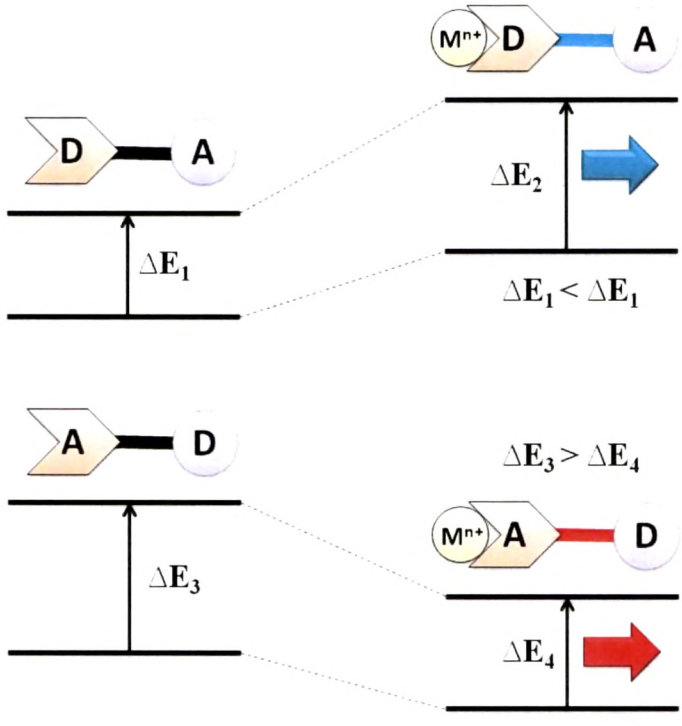

Figure 3.10. Schematic illustration for the PCT system.

Many fluorescent sensors have been designed according to the principle of PCT. Valeur *et al.* synthesized the compound **7** having an azacrown as the cation receptor containing a nitrogen atom which is conjugated to an electron-withdrawing group [34]. The compound 6 shows a common feature in which the blue shift of the absorption spectrum is much larger than that of the emission spectrum on cation binding (Ca^{2+}). Compound **8** undergo a large blue shift of the fluorescence spectrum upon cation binding (*see* Figure 3.11). **8** is one of the first crown-containing fluorescent PCT sensors that have been designed [35-37]. The fluorescence maximum shifts from 642 nm for the free ligand to 574 nm for the calcium complex in acetonitrile. The blue shift in case of compound **8** means there is no photodisruption of the interaction between the cation and the nitrogen atom of the crown which is in contrast to the compound **7**, because the nitrogen atom of the crown plays the role of a

second electron-donating atom with respect to the benzoxazinone moiety which is itself a donor–acceptor system. Metcalfe *et al.* reported a fluorescence-based receptor **9** in which the ionophore moiety has been specially designed for the determination of intracellular concentration of sodium ion [38]. An indole derivative was incorporated as fluorophore and upon binding to Na^+, the λ_{max} was shifted from 460 to 395 nm with FE of 25-fold. The large Stokes shift was proposed to be due to the formation of a TICT state.

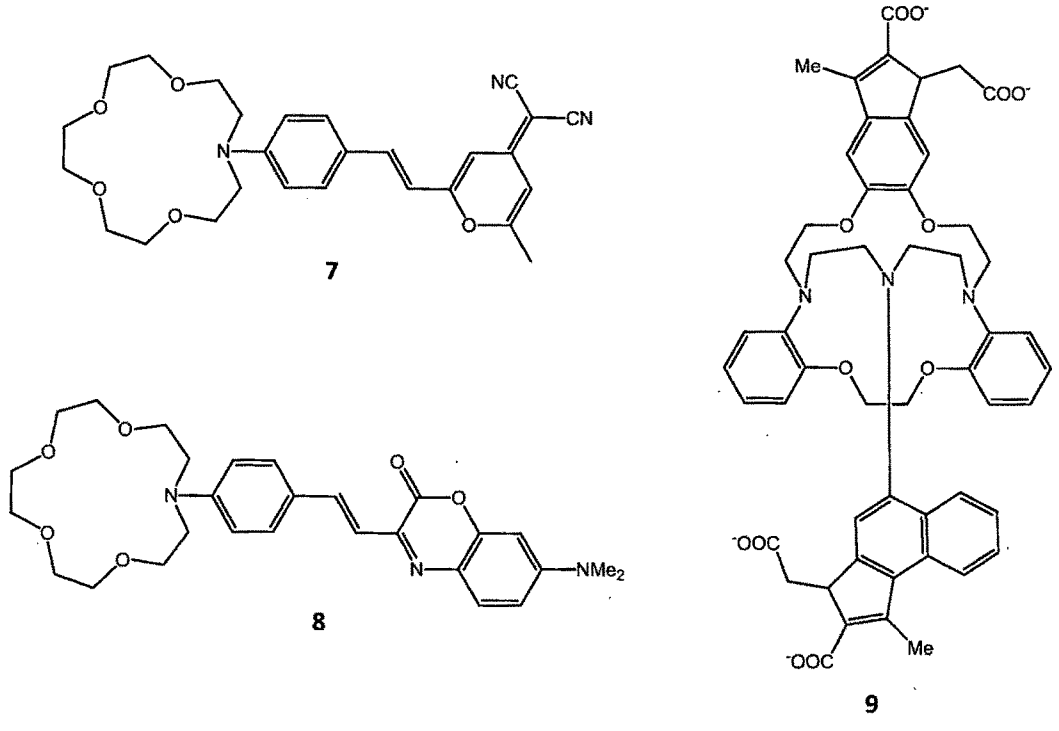

Figure 3.11. Structures of PCT based sensors.

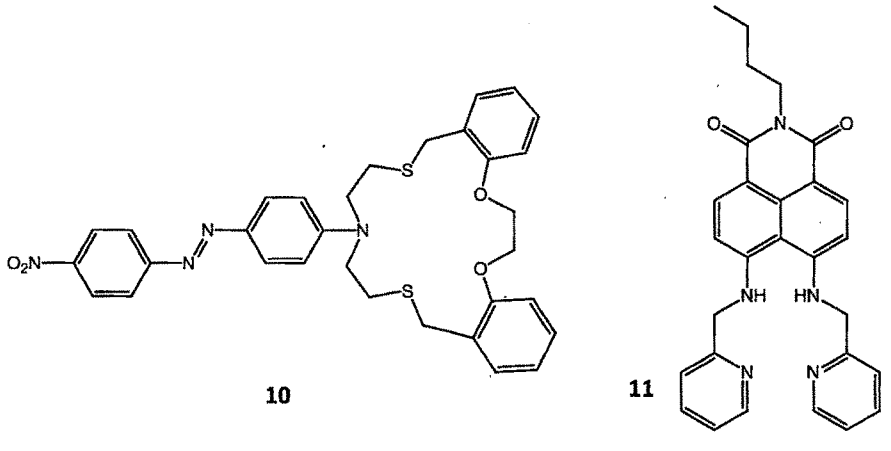

Figure 3.12. Structures of PCT based sensors.

Lee *et al* reported the N-azo coupled macrocycle **10** with a NO_2S_2 donor sites was selective towards Hg^{2+} ion [39]. Intense absorption band at 480 nm for compound **10** was blue shifted by 133 nm on binding to Hg^{2+} ion with a change in colour from red to pale-yellow. Crystal structure for this complex revealed that Hg^{2+} ion adopted a square planar geometry, where two S and one N atom arranged in an endo-fashion. Xu et al. also developed a 1, 8-naphthalimide based ratiometric fluorescent sensor **11**, where 4, 5-di[(pyridin-2-ylmethyl)amino] group was used as a selective binding pocket for Cu^{2+} ion [40] (*see* Figure 3.12). Binding to Cu^{2+} in aqueous ethanol solution induced the formation of a 1:1 complex, which exhibited a strong emission band with the λ_{max} of 475 nm at the expense of emission of **11** having λ_{max} at 525 nm.

3.1.3.5. Twisted Intramolecular Charge Transfer (TICT)

Relaxation towards an ICT state may be accompanied by internal rotation within the fluorophore. The prime example of great interest is 4-N,N-dimethylaminobenzonitrile (DMABN). This molecule exhibits dual fluorescence in polar solvents.

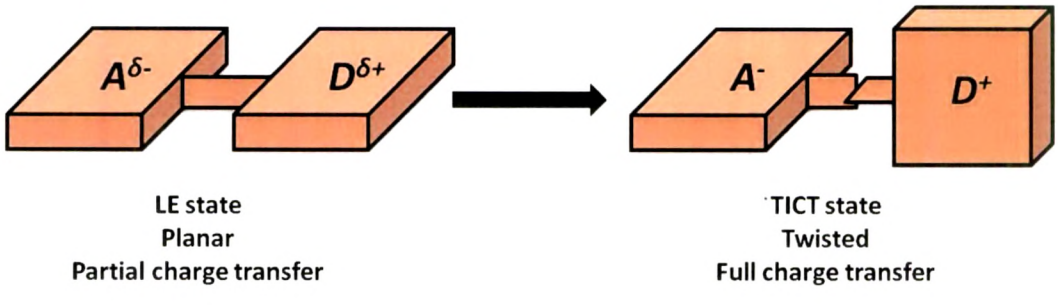

Figure 3.13. Representation of TICT model for DMABN [18].

This intriguing phenomenon can be explained as in the ground state the molecule is almost planar, which corresponds to the maximum conjugation between the dimethylamino group and the phenyl ring. According to the Franck-Condon principle, the locally excited state (LE) is still planar, but solvent relaxation takes place with a simultaneous rotation of the dimethylamino group until it is twisted at

right angles and the conjugation is lost. In the resulting TICT state, stabilized by the polar solvent molecules, there is a total charge separation between the dimethylamino group and the cyanophenyl moiety (*see* Figure 3.13).

3.1.4. Fluorescent chemosensors based on Rhodamine

The fluorescence of organic molecules depends sensitively on their environment. Fluorescent dyes have accordingly become popular molecular probes for the selective recognition of metal ions [6]. Among the fluorophores developed, Rhodamine derivatives are highly favourable because of their excellent photophysical properties, such as high extinction coefficients, excellent quantum yields, great photostability, and relatively long emission wavelengths [41]. Rhodamine was first synthesized by Noelting and Dziewonsky in 1905 [42] and has been widely used as fluorescent probes for the detection of various ions, in the lasing medium in dye lasers and fluorescent markers in biological studies [6, 41, 43]. The cation-sensing mechanism of these probes is based on the change in structure between spirocyclic and open-cycle forms. Without cations, probes exist in a spirocyclic form, which is less and nonfluorescent. Addition of metal cation leads to a spirocycle opening resulting in an appearance of pink and orange fluorescence. The additional advantage of such a rhodamine-based sensing system is that the ring-opening process is accompanied by a vivid change from less to pink, thus enabling the metal detection with the naked eye. In 1997 Czarnik and coworkers reported a pioneer work on the rhodamine B derivative and its ring opening mechanism for the selective recognition of Cu^{2+} ion [44].

In their study, rhodamine B hydrazide was used as a fluorescent chemodosimeter for Cu^{2+} ion. As illustrated in the Figure 3.14 Czarnik's rhodamine B hydrazide can recognize Cu^{2+} selectively, and Cu^{2+} promoted hydrolysis can provide fluorescent rhodamine B as a product. They demonstrated that this system can detect 10 nM Cu^{2+} within 2 min at pH 7. This work resulted in a great deal of attention being given to the application of the ring-opening processes of rhodamine B derivatives to fluorescent chemosensors. Many research groups have worked on the rhodamine-based fluorescent chemodosimeter and it is not possible to include all the examples of this kind in this chapter. However, we are providing some examples of rhodamine-

based fluorescent sensors for the detection of Cu^{2+}, Hg^{+}, Zn^{2+}, Pb^{2+}, Cr^{3+}, Fe^{3+} and Pd^{2+} in solutions.

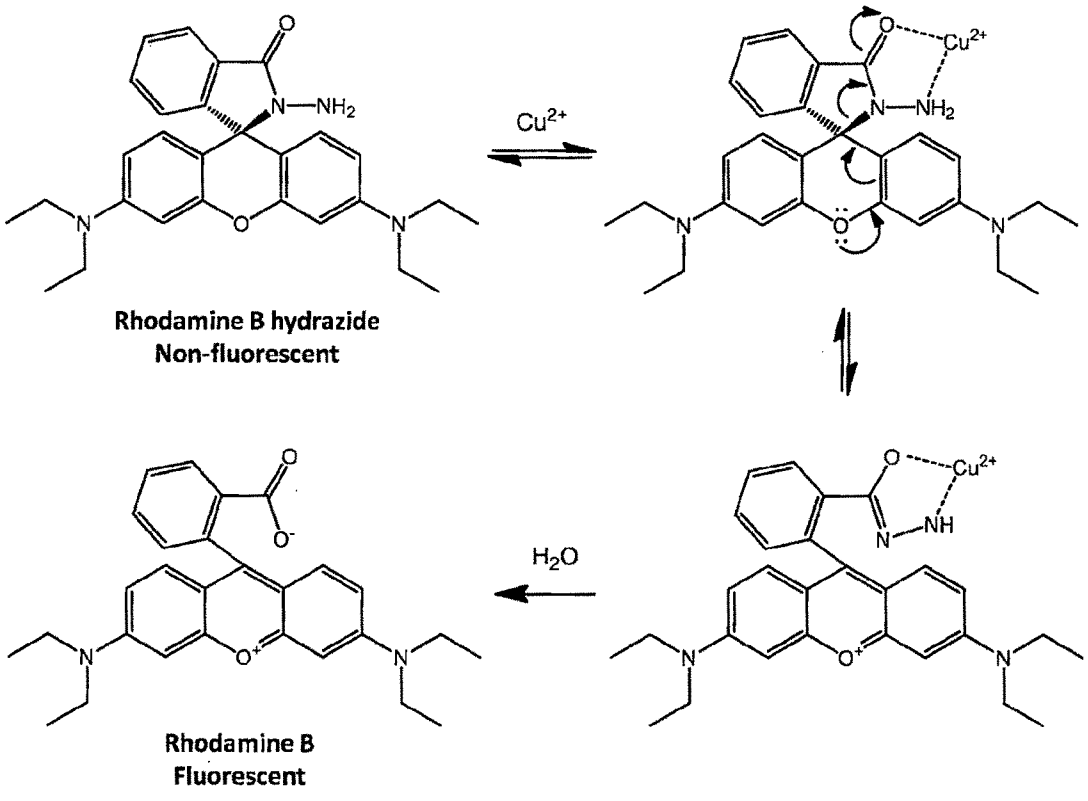

Figure 3.14. Complexation of Rhodamine B hydrazide with Cu^{2+} ion.

A rhodamine 6G derivative **12** was synthesized and used to detect Cu^{2+} in an aqueous medium [45]. Under optimized conditions, the quantification of Cu^{2+} by **12** using an absorptiometric method was satisfactory in the linear working range 0.05-5.00 μM, with a detection limit of 10 nM for Cu^{2+} and good tolerance of other metal ions. Kim and co-workers reported the design and synthesis of a new rhodamine-based derivative **13**, bearing an N-butyl-1,8naphthalimide group [46]. **13** displayed selective colorimetric and fluorescence "turn-on" changes at 550 nm via a rhodamine ring-opening approach toward Cu^{2+} ion (*see* Figure 3.15). It was reported that **13** forms 2:2 complex with Cu^{2+} ion. Zeng *et al* [47] reported 4-[{(E)-N-(rhodamine 6G lactam)-ethylenediamineimino}methyl]benzene-1,3-diol (**14**), which showed a reversible, selective, and sensitive fluorescence enhancement response to Cu^{2+} in HEPES buffer (20 mM, pH 7.0) containing 50% (v/v) CH_3CN. Mashraqui et al. [48] have synthesized a rhodamine 6G based chromo and fluorogenic probe **15**, which can detect micromolar concentrations of Zn^{2+} by turning the colour of the solution from

colourless to orange and also by changing the corresponding absorption maximum from 302 to 528 nm.

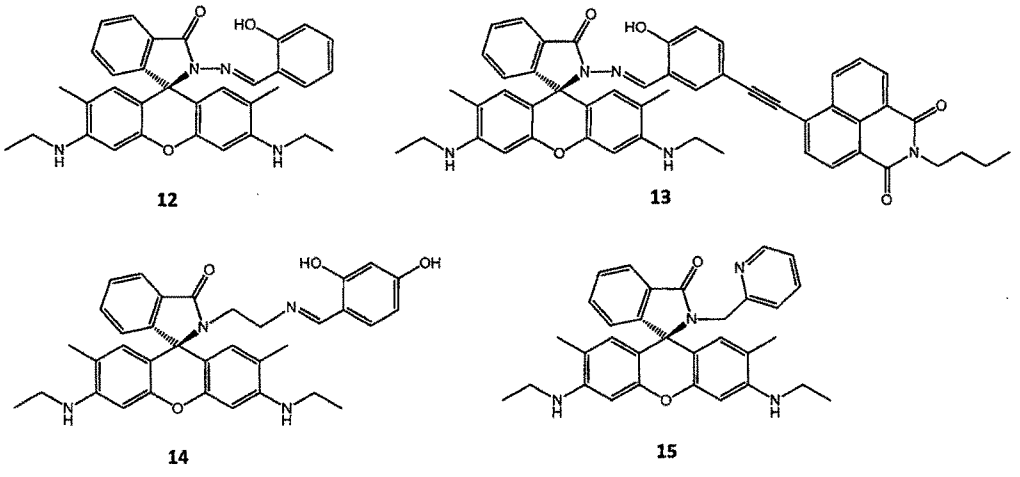

Figure 3.15. Structures of rhodamine 6G based fluorescent sensors.

Das et al. reported a rhodamine 6G based chemosensor **16** for the detection of Hg^{2+} and Cu^{2+} (*see* Figure 3.16). In water-methanol (1:1, v/v) solution at pH 7.0, both Hg^{2+} and Cu^{2+} induced colour changes with new absorption peaks appearing at 534 nm for Hg^{2+} and 528 nm for Cu^{2+} [49]. A 90-fold enhancement in fluorescence intensity at 554 nm was observed with the addition of only 8 equiv of Hg^{2+}, while no fluorescence change was found in the presence of Cu^{2+}, this was attributed to the quenching effect of paramagnetic copper ions.

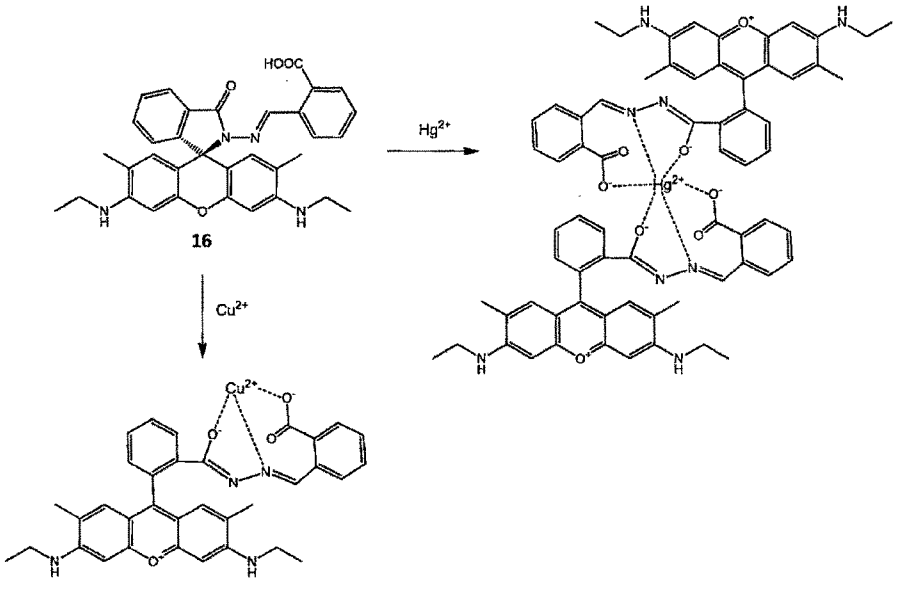

Figure 3.16. Binding mechanism of **16** with Hg^{2+} and Cu^{2+}.

Liu et al reported a rhodamine 6G based chemosensor **17**, showing Fe^{3+} induced fluorescence enhancement as a result of spirolactam ring-opening in aqueous solution [50]. The stoichiometry for the binding modes between **17** and Fe^{3+} were speculated to be 2:1 (*see* Figure 3.17).

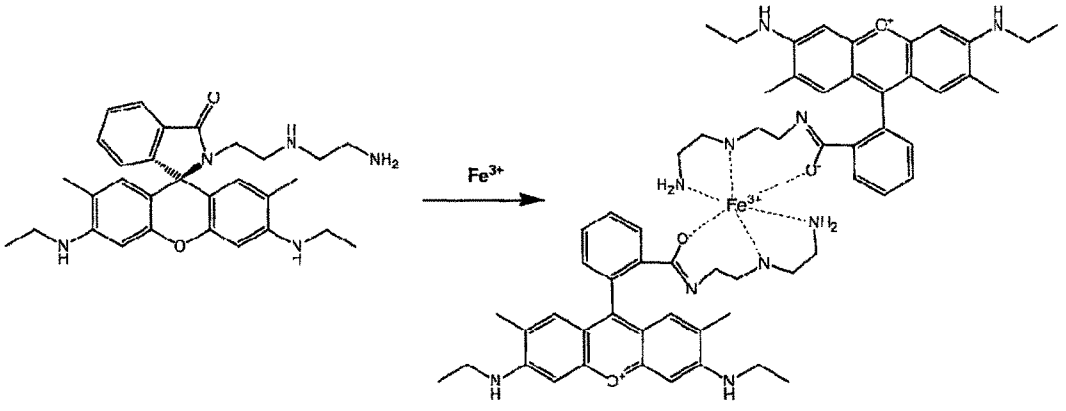

Figure 3.17. Binding mechanism of **17** with Fe^{3+}.

Kim et al. reported a sensor **18**, which consists of rhodamine as the main core and ethylenediamine as a spacer that links 2-hydroxy-5-nitrobenzaldehyde with the main core via a hydrolysable imine linkage [51]. The full moiety has been made in such a way that it may act as a Schiff base. Due to its high affinity toward the ethylenediamine framework, and being a strong Lewis acid, Fe^{3+} selectively binds with and facilitates hydrolysis of the Schiff base with concomitant opening of the spirocyclic ring, resulting in a red coloured solution and strong yellow fluorescence at 551 nm upon excitation at 528 nm in aqueous solutions. Tae et al. have developed rhodamine 6G based probe **19**, which has a flexible bis-aminoxy (diethylene glycol) multidentate binding unit for the detection of Fe^{3+} ions [52]. The probe exists predominantly as the spirocyclic form in H_2O-DMSO (99:1, v/v) and changes its colour rapidly from colourless to pink with a strong fluorescence that peaks at 557 nm (excitation at 500 nm) upon addition of Fe^{3+} ions to the solution (*see* Figure 3.18).

Compound **20** is a rhodamine 6G based chemosensor for the detection of Cr^{3+} at biological pH in aqueous solutions [50]. The possible mechanism for the binding of Cr^{3+} with **20**, involves a 1:1 stoichiometry. Lin et al. described rhodamine derivative **21** as a fluorescent sensor for the detection of gold ion through Au^{3+}-mediated hydrolysis of acylsemicarbazide to carboxylic acid [53]. Compound **21** displayed no fluorescence in PBS (pH 7.4, containing 0.3% DMF) due to it being in the spirocyclic

form. Upon addition of Au^{3+}, 132 exhibited a 233-fold enhancement in the fluorescence intensity.

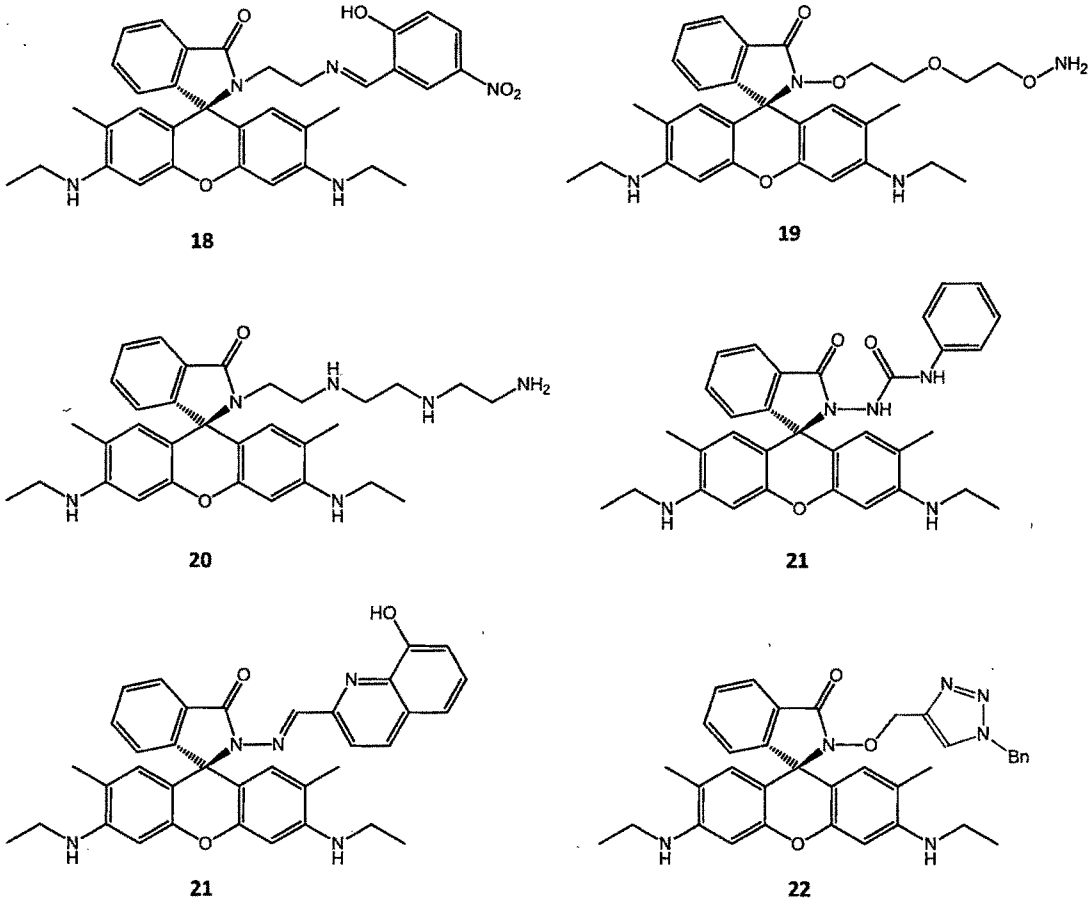

Figure 3.18. Structure of rhodamine 6G based fluorescent probes.

A sensitizing chromophore **22** containing the rhodamine 6G unit linked to 8-hydroxyquinoline-2-carboxaldehyde by a carbohydrazone linker, can donate its excitation energy in the visible range (~500 nm) to Yb^{3+}, which then emits near-infrared radiation at around 1000 nm [54]. Yb^{3+}, when coordinated with the rhodamine 6G moiety of **22**, induces spirolactam ring-opening of closed and nonfluorescent rhodamine 6G moieties to give the fluorescent ring-opened form, which has an absorption band maximum around 525 nm and an emission band maximum around 560 nm in acetonitrile. Tae et al. utilized a rhodamine 6G triazole as a fluorescent chemosensor for Pt^{2+} in aqueous solution [55]. The probe shows neither colour nor fluorescence in H_2O (DMSO, 1%, v/v), indicating that it exists predominantly in the spirocyclic form, as expected. Upon addition of Pt^{2+}, the probe

(5 μM) exhibits strong fluorescence at 562 nm as well as a colour change from colourless to pink-red in H_2O (DMSO, 1%, v/v).

3.1.5. Aim and outline of the present work

Selective detection of biologically important metal ions has tremendously gained its importance because metal ions are involved in a variety of fundamental biological processes in organisms. Iron is one of the most important metals in the biological systems and plays a key role in many biochemical processes at the cellular level. Specially, ferric ion (Fe^{3+}) is widely retained in many proteins and enzymes either for structural purposes or as part of a catalytic site [56]. Moreover, the ferric ion is well-known as a fluorescence quencher due to its paramagnetic nature, and most of the reported Fe^{3+} receptors, such as analogues of ferrichromes or siderophores, undergo a fluorescence quenching when bound with Fe^{3+} [57], though it is usually believed that probes with a fluorescence enhancement signal when interacting with analytes are much more efficient. Therefore, the development of new fluorescent indicators for accurate and specific detection of Fe^{3+}, especially those that exhibit selective Fe^{3+} -amplified emission, is still a challenge. Recently, a few sensors have been described to exhibit a turn-on response to Fe^{3+} ions [51, 58].

Pyrazolone, as a prominent structural motif, is found in numerous active compounds. Due to its easy preparation and its rich biological activity, pyrazolone and its metal complexes have received considerable attention in coordination chemistry and medicinal chemistry [59]. 4-formyl derivatives of pyrazolones can form a variety of Schiff bases and are reported to be superior reagents in various biological applications [60]. A literature servey shows that only a few attempts have been made for the synthesis of fluorescent sensors containing pyrazolone as a recognition moiety for metal ions [61]. However, to the best of our knowledge, there is no example of a fluorescent sensor for the metal ion using a Schiff base of rhodamine 6G and 4-formyl derivatives of pyrazolones. In this chapter, we have synthesized two rhodamine 6G based fluorescent molecular sensors using 5-hydroxy-3-methyl-1-phenyl-1H-pyrazole-4-carbaldehyde and 5-hydroxy-3-methyl-1-(p-tolyl)-1H-pyrazole-4-carbaldehyde as the recognition moieties.

3.2. Experimental

3.2.1. Materials and physical measurments

All chemicals and solvents involved were of analytical grade. Dry N,N'-dimethylformamide (DMF) was purchased from Merk. Solvents for spectral studies were freshly purified by standard procedures. The compounds 5-hydroxy-3-methyl-1-phenyl-1H-pyrazole-4-carbaldehyde (**1a**) and 5-hydroxy-3-methyl-1-p-tolyl-1Hpyrazole-4-carbaldehyde (**1b**) were synthesized following method reported in Part **3** of Chapter **1**. Compound **2** was synthesized following as reported in the literature [62]. All metal nitrate salts were purchased from Sigma-Aldrich. Rhodamine 6G and ethylenediamine were purchased from Spectrochem. 3-Methyl-1-toluoyl-5-pyrazolone and 3-methyl-1-phenyl-5-pyrazolone were obtained from Nutan Dye Chem, Surat.

^{1}H and ^{13}C NMR spectra were recorded with Avance-III 400 MHz Bruker FT-NMR instrument. Elemental analyses of C, H, and N were determined using a Perkin Elmer series-II 2400 elemental analyser. FT-IR spectra were recorded as the KBr pellet on the Perkin Elmer Fourier transform (FT-IR) spectrum RX 1 spectrometer. Mass spectra were recorded on a Q-TOF Micro™ LC-MS instrument. The UV/Vis spectra were recorded on a CARY 500 Scan UV–Vis–NIR spectrophotometer (Varian). Emission spectra were recorded using an Edinburgh Instruments model Xe-900.

3.2.2. Synthesis of chemosensors L^1 and L^2

Synthesis of L^1

Ligand L^1 and L^2 were synthesized from **2**. Compound **2** (0.184 g, 0.4 mmol) was dissolved in hot methanol (30 ml). Then, 5-hydroxy-3-methyl-1-phenyl-1H-pyrazole-4-carbaldehyde (0.081 g, 0.4 mmol) was added. The reaction mixture was stirred and heated to reflux for 4 h, after which it was cooled and filtered. The solid mass was washed with methanol and dried to afford L^1 as an off-white solid: 0.158 g (60.3%); ^{1}H NMR ($CDCl_3$, 400 MHz), δ 1.3-1.34 (*t*, J = 7.2 Hz, 6H), 1.88 (*s*, 6H), 2.19 (*s*, 3H), 3.19-3.34 (*m*, 8H), 3.52 (*br*, 2H, -NH), 6.20 (*s*, 2H), 6.38 (*s*, 2H), 7.07-7.12 (*m*, 2H), 7.35-7.39 (*m*, 2H), 7.49-7.51 (*m*, 2H), 7.95-7.99 (*m*, 2H), 9.33 (*s*, 1H) ppm; ^{13}C NMR (400 MHz CDCl3): δ 12.64, 14.69, 16.72, 38.33, 40.65, 46.94, 65.28,

96.54, 100.73, 105.22, 118.26, 118.46, 122.94, 123.88, 123.99, 128.14, 128.31, 128.65, 130.75, 132.93, 139.26, 147.65, 147.80, 151.41, 151.73, 153.39, 165.62, 168.63 ppm; Elemental analyses (%): found: C 73.15, H 6.34, N 13.13; calcd: C 73.10, H 6.29, N 13.12. LC-MS (m/z): 640.51 $[M]^+$.

Synthesis of L^2

Compound **2** (0.184 g, 0.4 mmol) was dissolved in hot methanol (30 ml). Then, 5-hydroxy-3-methyl-1-p-tolyl-1Hpyrazole-4-carbaldehyde (0.086 g, 0.4 mmol) was added. The reaction mixture was stirred and heated to reflux for 2 h, after which it was cooled and filtered. The solid mass was washed with methanol and dried to afford L^2 as off-white solid: 0.166 g (64.8%); ^{1}H NMR ($CDCl_3$, 400 MHz), δ 1.30-1.33 (*t*, J = 7.2 Hz, 6H), 1.88 (s, 6H), 2.19 (s, 3H), 2.34 (*s*, 3H), 3.19-3.33 (*m*, 8H), 3.52 (*br*, 2H, -NH), 6.20 (*s*, 2H), 6.37 (*s*, 2H), 7.07-7.09 (*m*, 1H), 7.16 (*d*, 8.4 Hz, 2H), 7.49-7.51 (*m*, 2H), 7.84 (*d*, 8.4 Hz, 2H), 7.95-7.97 (*m*, 1H), 9.31 (*s*, 1H) ppm; ^{13}C NMR (400 MHz CDCl3): δ 12.62, 14.69, 16.71, 20.94, 65.28, 96.54, 100.77, 105.22, 118.25, 122.93, 123.99, 128.14, 128.30, 129.18, 130.76, 132.92, 133.36, 136.84, 147.53, 147.65, 151.33, 151.73, 153.39, 165.43, 168.61 ppm; Elemental analyses (%): found: C 73.42, H 6.53, N 12.85; calcd: C 73.37, H 6.47, N 12.83. LC-MS (m/z): 654.64 $[M]^+$.

3.2.3. Ion binding study

Stock solutions of compounds L^1 and L^2 (2×10^{-5}M) were prepared by dissolving the compounds in acetonitrile-aqueous (50:50). Solutions of nitrate salts (2×10^{-4}M) of various cations (Na^+, K^+, Ag^+, Ni^{2+}, Co^{2+}, Cu^{2+}, Ca^{2+}, Zn^{2+}, Cd^{2+}, Hg^{2+}, Pb^{2+}, Fe^{3+}, Cr^{3+} and Al^{3+}) were prepared in acetonitrile-aqueous solution. Then 2 mL of a stock solution of L^1/ L^2 and 2 mL of a stock solution of each metal salt added to a 5 mL volumetric flask, so that the effective concentration of compounds L^1 and L^2 was 1×10^{-5} M and that of the metal ions was 1×10^{-4}M (10 equivalent). The luminescence spectra of the resulting solutions and of the original compounds (1×10^{-5} M) were recorded on excitation at the absorption maxima (λ_{max}) 530 nm. The spectra of the cation-containing solutions were compared with that of the original solution to ascertain the interactions of the cations with the ionophore. The UV/Vis spectra of all solutions containing metal ions (10 equivalents) were also recorded. Metal ions that exhibited substantial changes in absorption and emission intensities

were considered for the absorption and emission titrations to determine the association constant. For the emission titration study, the same stock solutions of the compounds L^1 and L^2 were used and a solution of the nitrate salts of the selected metal ions (Fe^{3+}, Al^{3+} and Cr^{3+}) of the desired concentration (2×10^{-5} - 2×10^{-3} M) were prepared by proper dilution of the stock solution. Then, 2 mL of each solution were mixed in a 5 mL volumetric flask to prepare the reaction mixture with 0.1–100 M equivalents of the metal ion with respect to the concentration of the complexes; the luminescence spectra of the resulting solutions were recorded.

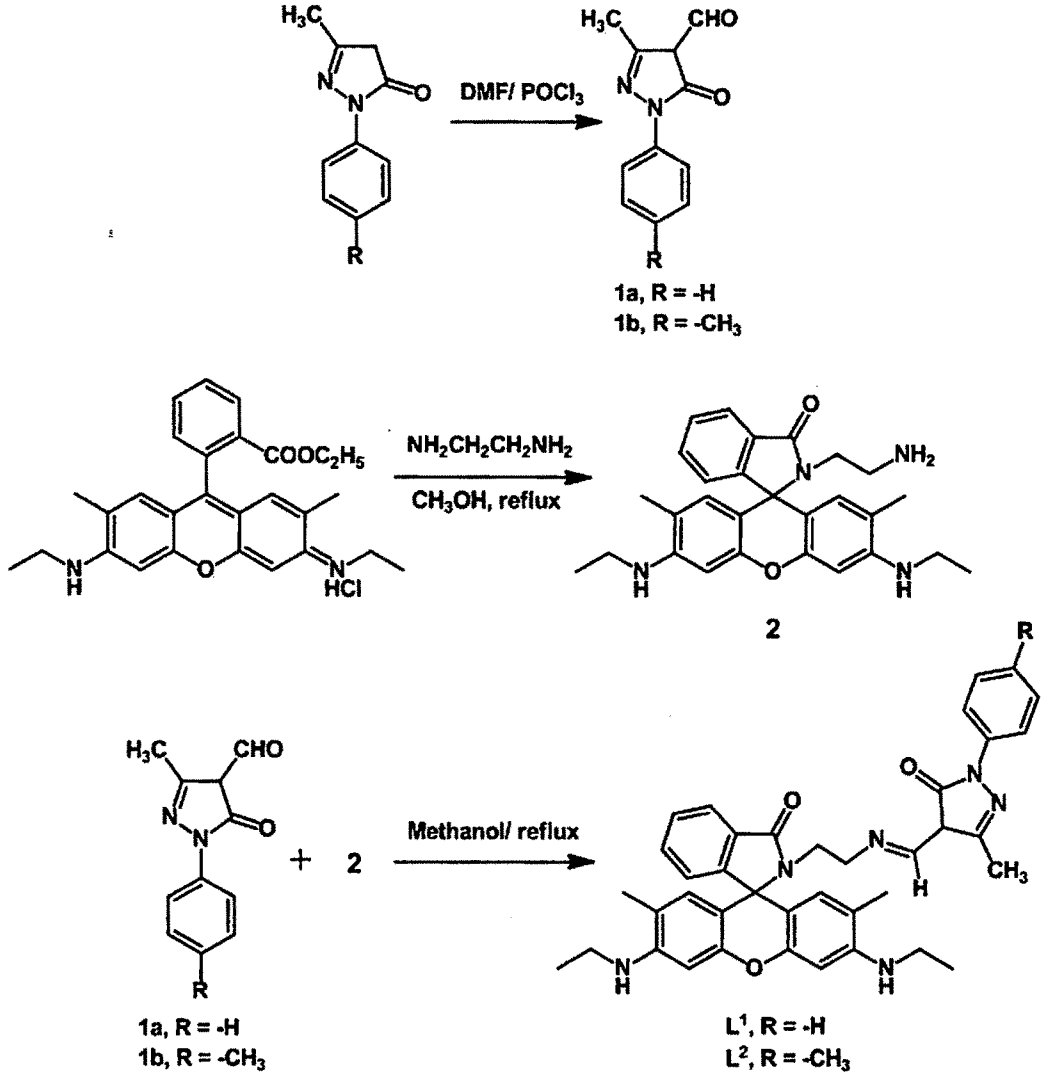

Scheme 3.1. Synthesis of L^1 and L^2.

3.3. Results and Discussion

3.3.1. Syntheses and characterizations

The synthetic route for the compounds L^1 and L^2 is shown in Scheme 3.1. The compounds L^1 and L^2 were synthesized by the reaction of intermediate **1a** and **1b** with **2**. All the compounds were characterized on the basis of analytical and spectroscopic data. Elemental analyses and mass spectrometric data are in excellent agreement with the calculated values for the proposed structures of the compounds. **1a** and **1b** were synthesized by the condensation of 3-methyl-1-phenyl-2-pyrazolin-5-one and 3-methyl-1-toluoyl-5-pyrazolone with DMF and $POCl_3$, respectively. Compound **2** was synthesized by refluxing the mixture of rhodamine-6G and ethylenediamine in ethanol. The reaction mixture was refluxed until the fluorescence of the solution disappeared. The disappearance of fluorescence indicats the formation of spirolactam ring in the compound **2**. The ^1H NMR spectra of L^1 and L^2 are shown in Figure 3.19 and Figure 3.20.

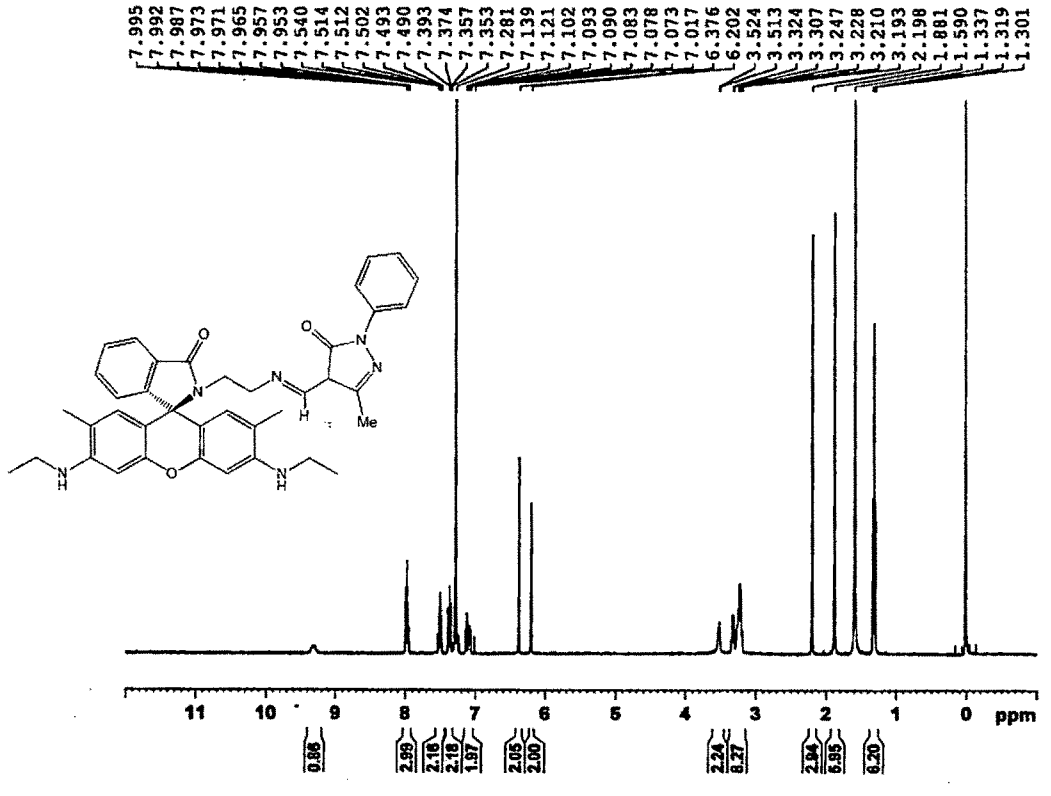

Figure 3.19. ^1H NMR spectrum of L^1.

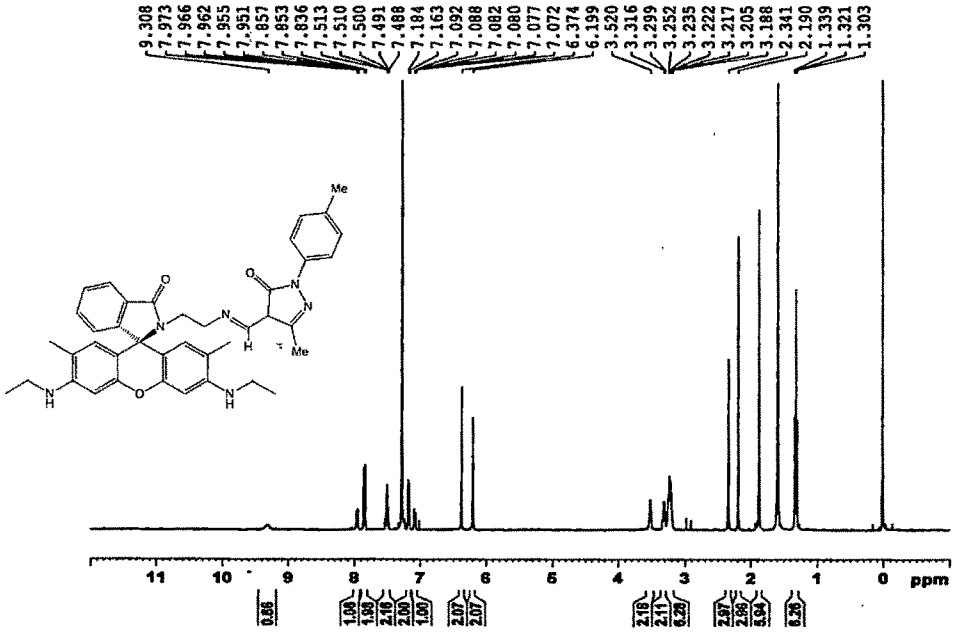

Figure 3.20. ^{1}H NMR spectrum of L^{2}.

Meanwhile, the characteristic peak at 65.28 ppm in the ^{13}C NMR spectrum also supports the existence of spirolactam form. Condensation of compound **2** with 4-fomyl derivative of pyrazolone (**1a** and **1b**) produces L^{1} and L^{2}, respectively. The ^{13}C NMR spectra of L^{1} and L^{2} are shown in Figure 3.21 and Figure 3.22.

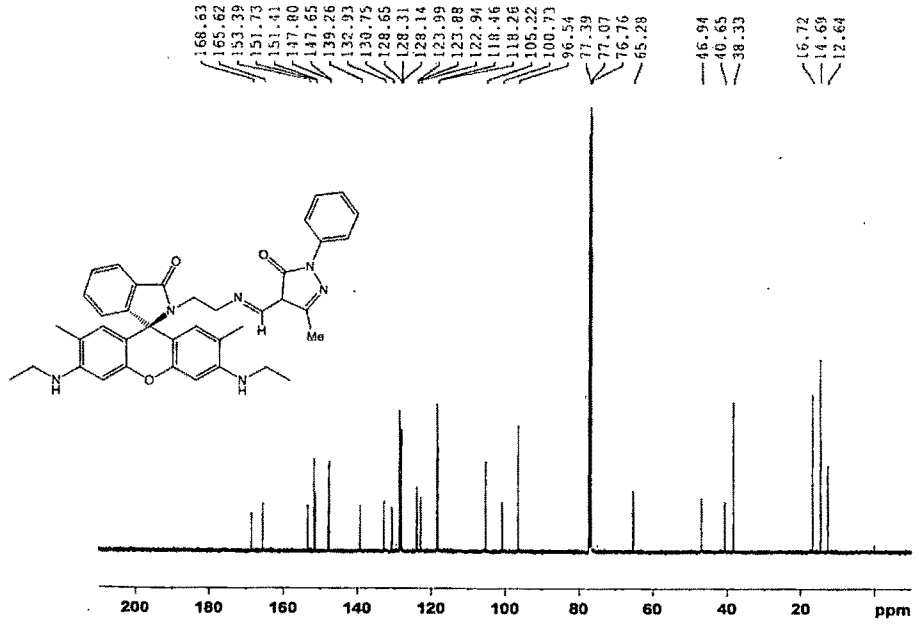

Figure 3.21. ^{13}C NMR spectrum of L^{1}.

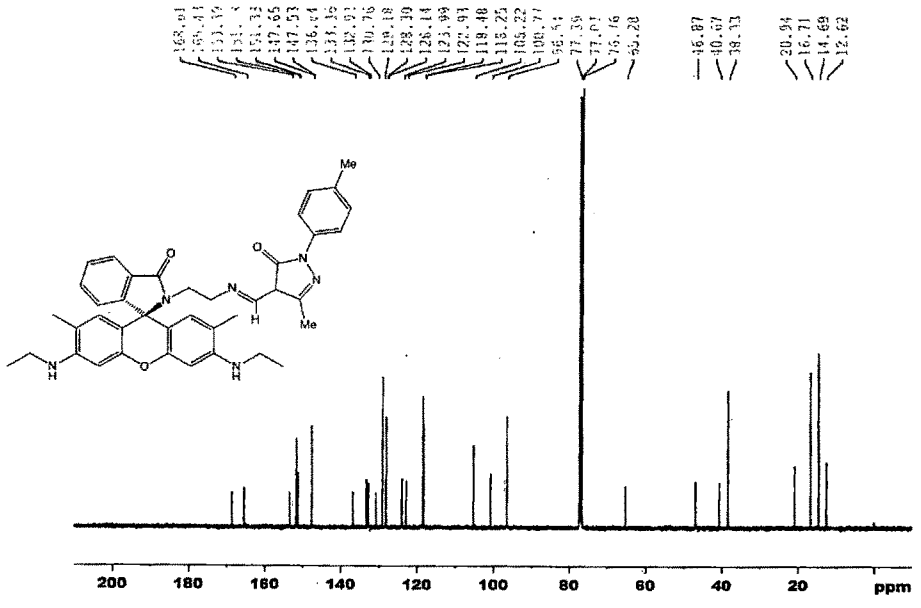

Figure 3.22. ^{13}C NMR spectrum of L^2.

The mass spectrum of L^1 shows molecular ion peak $[M]^+$ at 640.51, $[M+Na]^+$ peak at 663.5 and $[M+K]^+$ peak at 679.51, which are in good agreement with the proposed structure for the L^1. Mass spectrum of L^2 shows molecular ion peak $[M]^+$ at 654.6, $[M+H]^+$ peak at 655.9 and $[M+Na]^+$ at 677.67, which agreed well with the proposed structure. Mass spectra of L^1 and L^2 are presented in the Figure 3.23 and Figure 3.24.

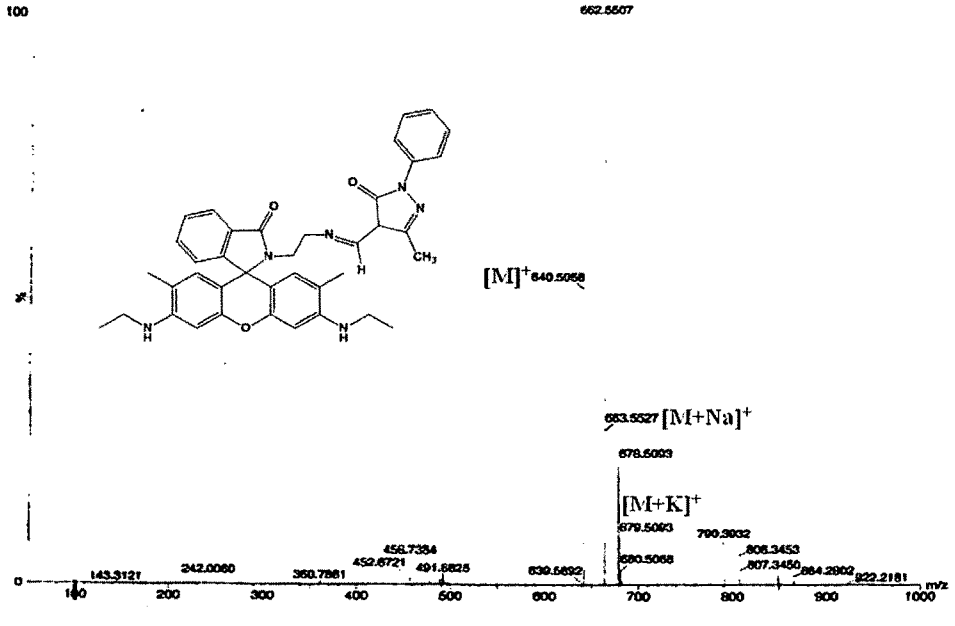

Figure 3.23. LC-MS of L^1.

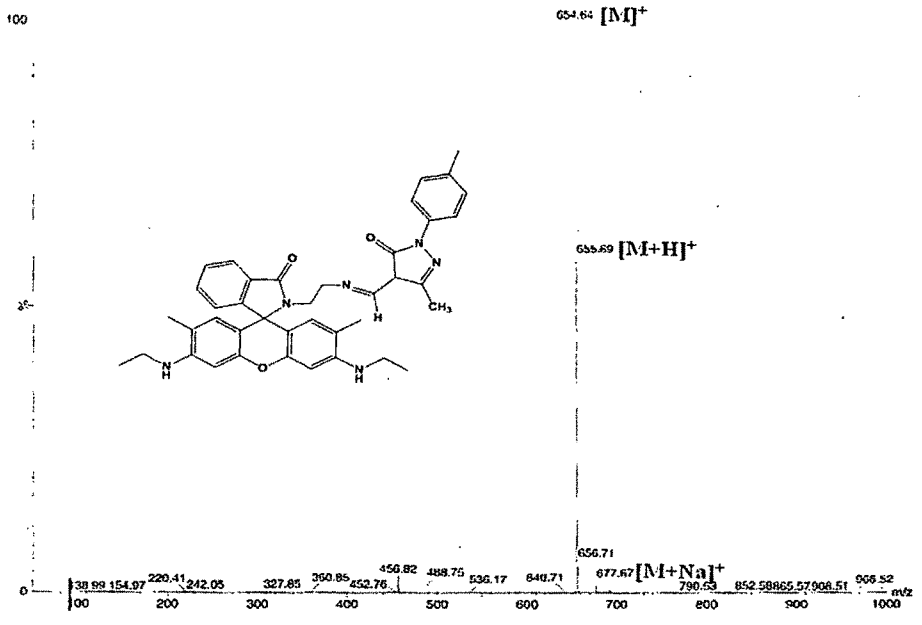

Figure 3.24. LC-MS of L^2.

The fluorescence and UV-Vis spectra of both the fluoroionophores (L^1 and L^2) were recorded in acetonitrile-aqueous (1:1) at room temperature. Compounds L^1 and L^2 are insoluble in water and generally, the metal ions containing samples are in the aqueous medium. Thus, we chose an acetonitrile-water mixture for better solubility of the compounds and their applicability to the aqueous samples. Compounds L^1 and L^2 in acetonitrile-aqueous were nonfluorescent, indicating that spirolactam form exist predominantly. Earlier reports reveal that certain transition-metal ions bind selectively with appropriate derivatives of rhodamine, where metal-ion binding induces opening of the spirolactam ring and generation of the xanthene form, with associated changes in the electronic and fluorescence spectral patterns. Thus, we checked the binding affinity of L^1 and L^2 toward all common metal ions, e.g. Na^+, K^+, Ag^+, Ni^{2+}, Co^{2+}, Cu^{2+}, Ca^{2+}, Zn^{2+}, Cd^{2+}, Hg^{2+}, Pb^{2+}, Fe^{3+}, Cr^{3+} and Al^{3+} (10 equivalent) by observing changes in the electronic and fluorescence spectral patterns in an acetonitrile-medium. The spectral changes for L^1 and L^2 upon addition of various metal ions are shown in Figure 3.25 and 3.26.

After the addition of metal ions, UV/vis absorption spectra showed a distinct change and the appearance of a new spectral band with a maximum at 530 nm for Fe^{3+} ions. The absorption band at 530 nm in the case of Fe^{3+} is due to the formation of delocalized xanthane moiety of rhodamine by selective Fe^{3+}-induced ring opening of

spirolactam, which also explains the change in color from colorless to pink in the presence of this Fe^{3+} ion. Without metal ions L^1 and L^2 show almost no fluorescence upon excitation at 530 nm, suggesting that L^1 and L^2 exist in a ring closed nonfluorescent spirolactam conformation. The addition of Fe^{3+} creates strong fluorescence upon excitation at 530 nm, indicating strong complexation of Fe^{3+} with L^1 and L^2. In other words, free L^1 and L^2 were non-emissive, but their fluorescence can turn from "off" to "on" when Fe^{3+} ions were added.

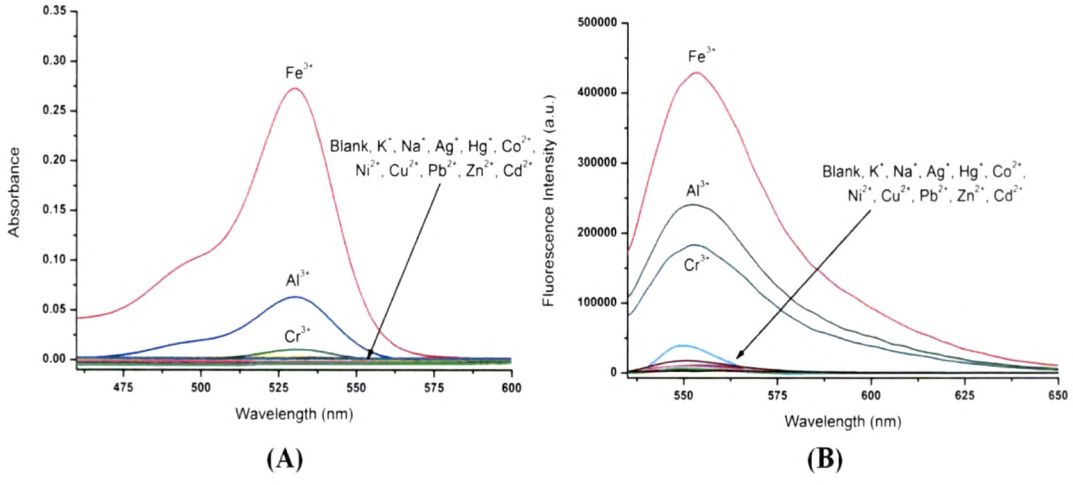

(A) **(B)**

Figure 3.25. (A) The absorption change and (B) the fluorescence intensity change profile of L^1 to different metal ions (10 equivalent) in acetonitrile-water (1:1).

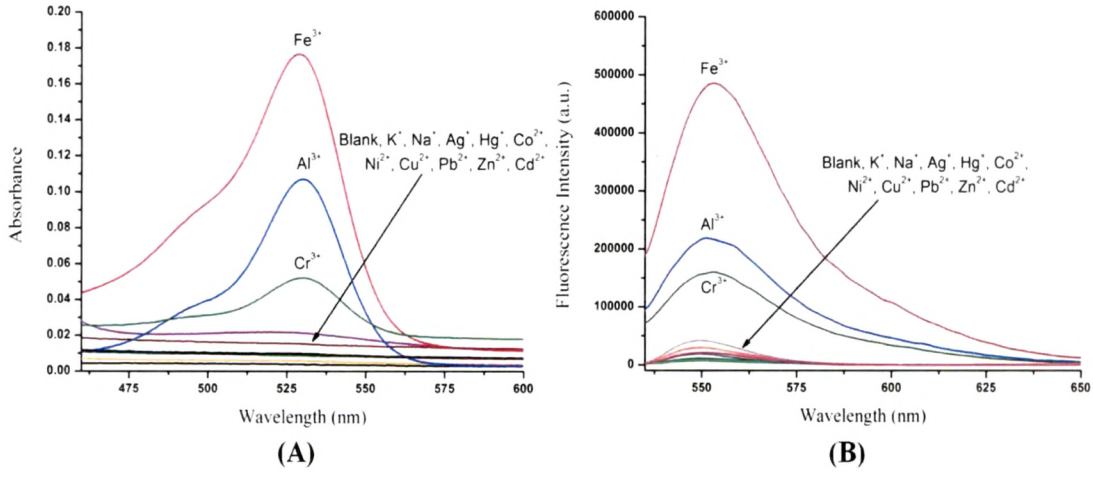

(A) **(B)**

Figure 3.26. (A) The absorption change and (B) the fluorescence intensity change profile of L^2 to different metal ions (10 equivalent) in acetonitrile-water (1:1).

However, L^1 and L^2 also show weak absorption and emission intensities with Al^{3+} and Cr^{3+} ions. For Fe^{3+} spectral changes were also associated with a visually detectable change from colorless to pink-red, no such change could be detected visually for any of the other cations studied.

3.3.2. Stoichiometry and binding mode study

To elicit the interaction between L^1, L^2 and Fe^{3+}, the UV-Vis and fluorescence spectral variation in L^1 and L^2 (2×10^{-5} M) in acetonitrile-aqueous were titrated with different concentration of Fe^{3+}. The UV-Vis titration experiments of L^1 and L^2 in acetonitrile-aqueous solution are shown in Figure 3.27 and 3.28. Upon gradual addition of Fe^{3+}, the titration experiment shows a sharp increase in the band at 530 nm. The appearance of the band at 530 nm might be due to the coordination of imine nitrogen atom of the L^1 and L^2 with the Fe^{3+} ions. In the fluorescence titration experiment shown in the Figures 3.28, upon gradual addition of Fe^{3+} ions, the ring opened rhodamine emission band at 556 nm is enhenced. The rhodamine emission band at 556 nm attained saturation at an Fe^{3+} concentration of ~ 6.0×10^{-4} M (60 equiv. of Fe^{3+}).

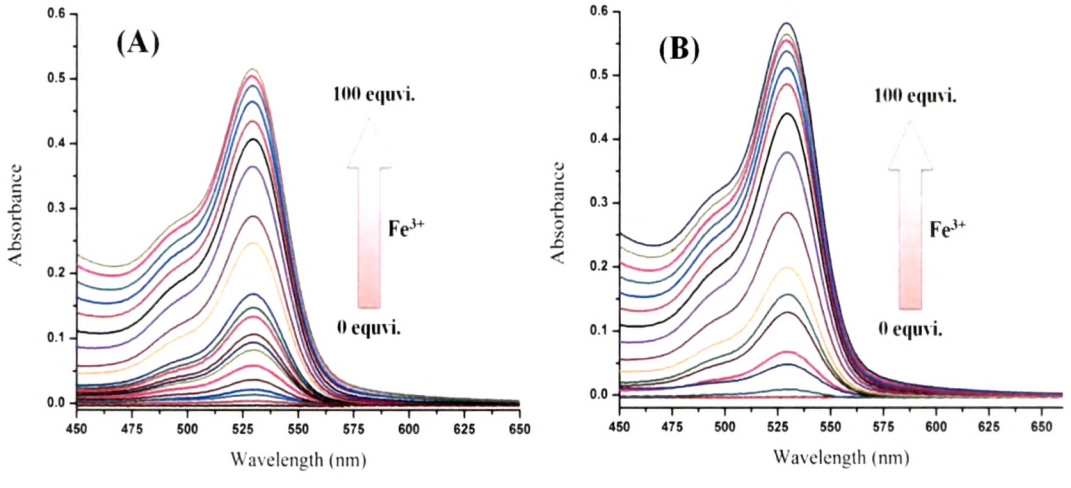

Figure 3.27. (A) UV-Vis titration profile of L^1 (2×10^{-5}M) in the presence of Fe^{3+} ions (0-100 equiv.) in acetonitrile-water (1:1 v/v). (B) UV-Vis titration profile of L^2 (2×10^{-5}M) in the presence of Fe^{3+} ions (0-100 equiv.) in acetonitrile-water (1:1 v/v).

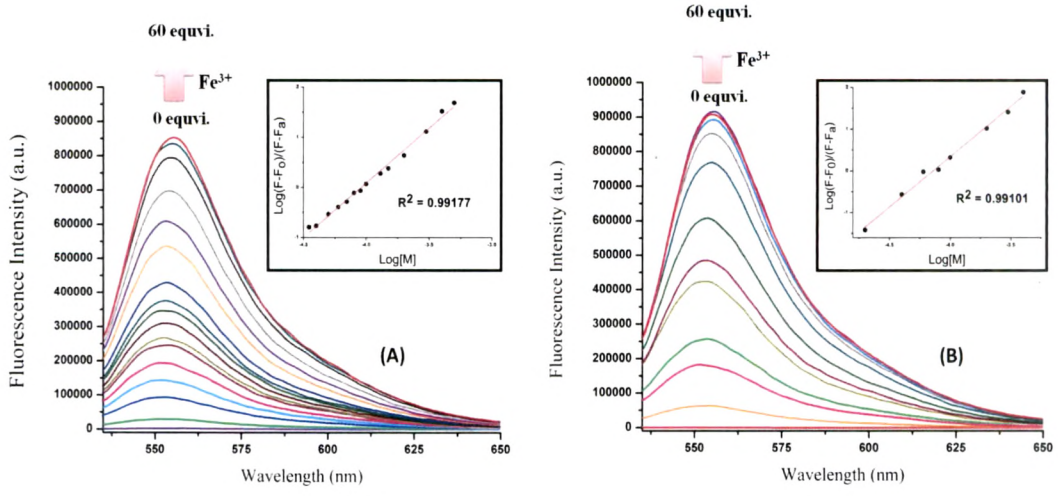

Figure 3.28. (A) Fluorescence titration profile of L^1 (2 x 10^{-5}M) in the presence of Fe^{3+} ions (0-60 equiv.) in acetonitrile-water (1:1 v/v) (λ_{exc} = 530 nm). Inset: linear regression fit (double-logarithmic plot) of the titration data as a function of the concentration of the metal ion. (B) Fluorescence titration profile of L^2 (2 x 10^{-5}M) in the presence of Fe^{3+} ions (0-60 equiv.) in acetonitrile-water (1:1 v/v) (λ_{exc} = 530 nm). Inset: linear regression fit (double-logarithmic plot) of the titration data as a function of the concentration of the metal ion.

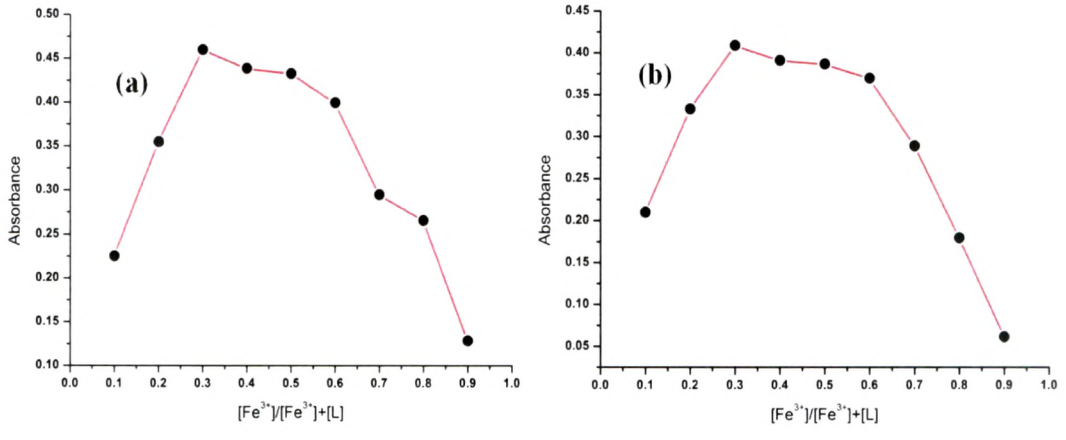

Figure 3.29. Job plots of (a) L^1 with Fe^{3+} in acetonitrile-water (50-50) and (b) L^2 with Fe^{3+} in acetonitrile-water (50-50).

The Job plot with respect to 530 nm showed that the absorbance attained a maximum at a molar fraction of ~ 1/3, indicating that a 1 : 2 stoichiometry was most likely for the binding of Fe^{3+} with L^1/ L^2 (*see* Figure 3.29). It is found in the literature

that the majority of rhodamine based fluorescent chemosensors show a 1:1 binding stoichiometry of Fe^{3+} and fluorescent chemosensors [41, 58*d*, 63]; there are only a few reports of the 1:2 binding of Fe^{3+} and fluorescent chemosensors [50,64]. In the fluorescent chemosensors described here, binding stoichiometry is 1:2 for Fe^{3+} and L^1/L^2. The two rhodamine-pyrazolone ligands attach one metal ion of Fe^{3+}. The Job plots for Al^{3+} and Cr^{3+} indicate 1:1 stoichiometry with compounds L^1 and L^2 (*see* Figure 3.30).

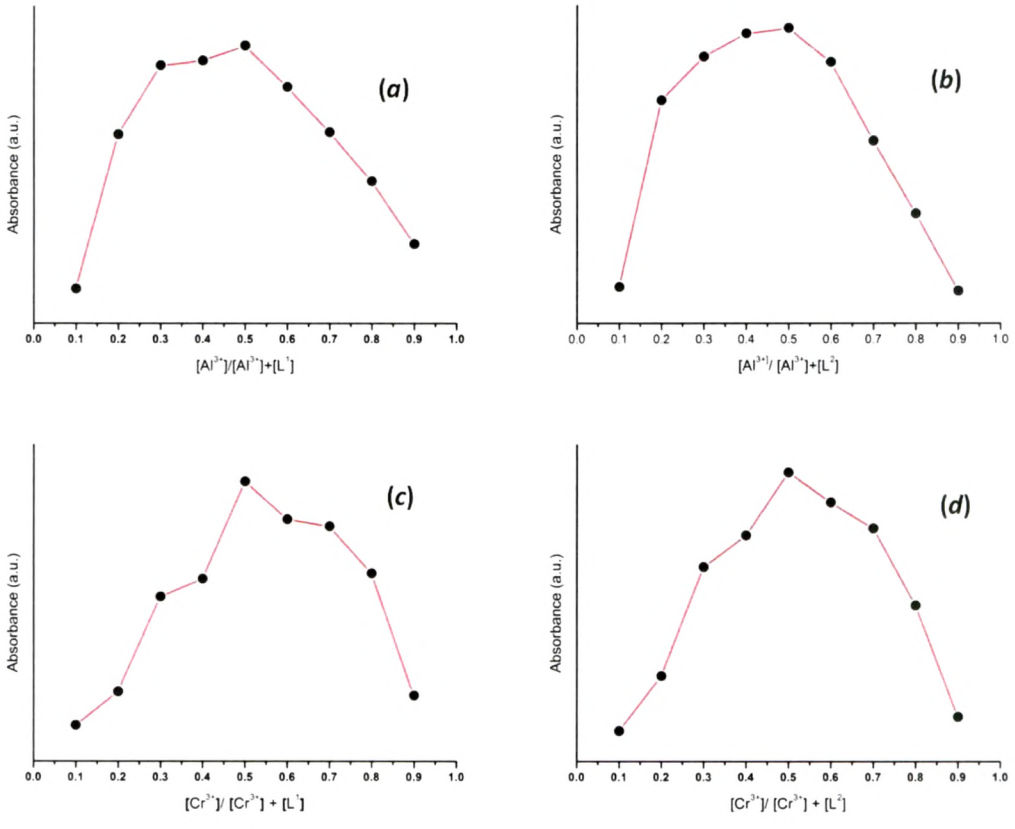

Figure 3.30. Jobs plot showing 1:1 binding stoichiometry of (*a*) Al^{3+} with L^1, (*b*) Al^{3+} with L^2, (*c*) Cr^{3+} with L^1 and (*d*) Cr^{3+} with L^2.

From the absorption titration experiment, the association constant for Fe^{3+} and L^1 was estimated to be 6.08×10^5 M^{-2} on the basis of non-linear fitting of the titration curve [65] assuming 1 : 2 stoichiometry (*see* Figure 3.31). The association constant for Fe^{3+} and L^2 was estimated to be 4.10×10^6 M^{-2} (*see* Figure 3.32). The association constants for the chemosensors L^1 and L^2 are higher than the reported values [64*a*], indicating that L^1 and L^2 bind more strongly than the reported chemosensors [64*a*] with Fe^{3+}. The detection limit of L^1 and L^2 were also calculated as 6.1×10^{-6} M and

4.2×10^{-6} M, respectively, from the fluorescence titration data [66]. The higher selectivity of compounds towards Fe^{3+} ions might be because the electrode potential of Fe^{3+} is greater than that of Al^{3+} ions [66]. The binding stoichiometry of Fe^{3+} with L^1 and L^2 is 1:2, leading to greater enhancement of the absorption and emission bands in comparison with Al^{3+} and Cr^{3+}, which show 1:1 binding stoichiometry.

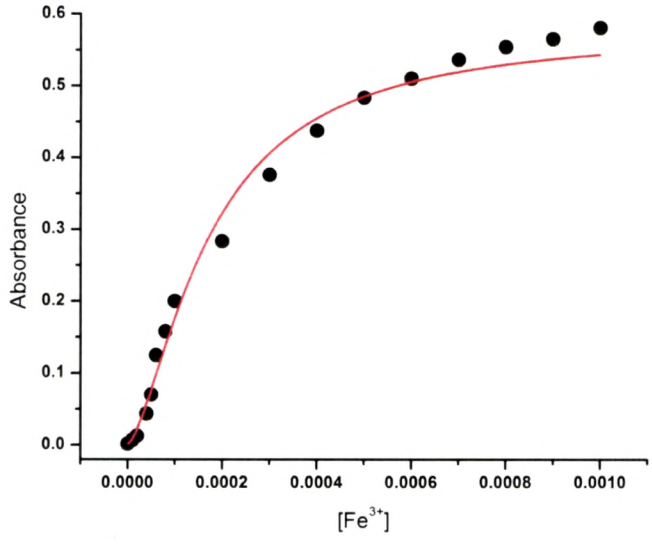

Figure 3.31. UV-Vis titration profile of L^1 (2×10^{-5} M) in CH_3CN/H_2O solution (1:1, v/v), from which the association constant was determined, Ka = 6.08×10^5 M^{-2} (R^2 = 0.9896).

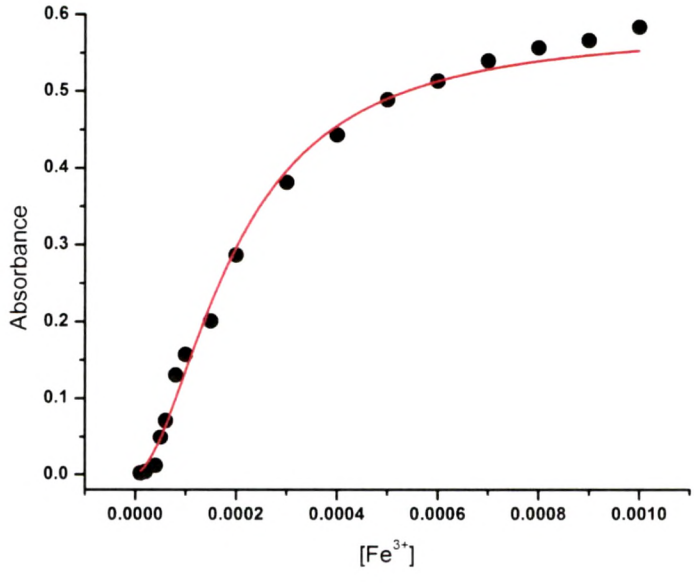

Figure 3.32. UV-Vis titration profile of L^2 (2×10^{-5} M) in CH_3CN/H_2O solution (1:1, v/v), from which the association constant was determined, Ka = 4.10×10^6 M^{-2} (R^2 = 0.9938).

Thus, considering the Job plots and association constants in accordance with 1:2 stoichiometry, the possible binding mode between L^1 or L^2 and Fe^{3+} is proposed in scheme 3.2.

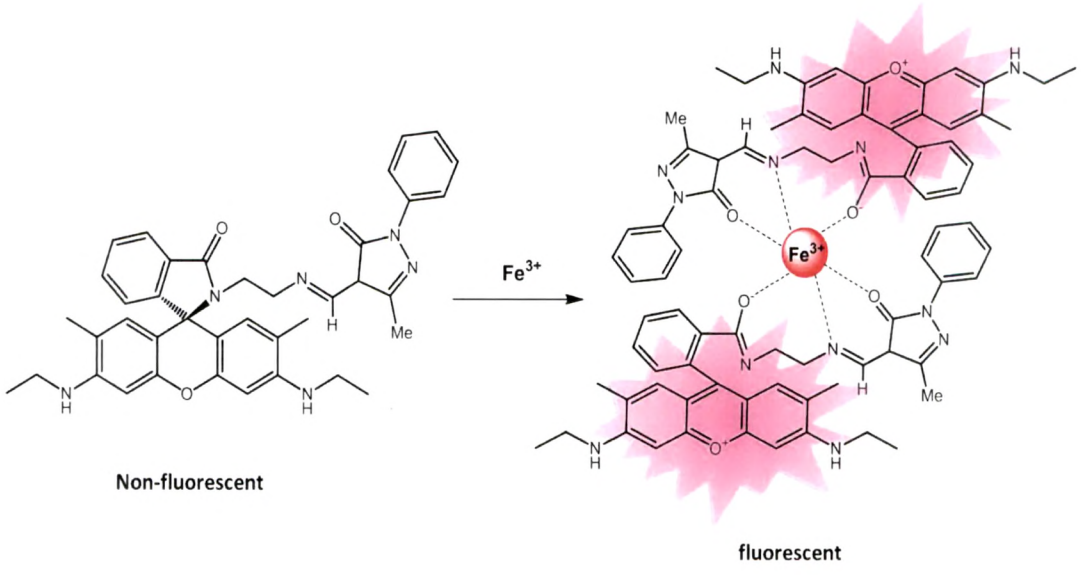

Scheme 3.2. Proposed binding structure of L^1 with Fe^{3+}.

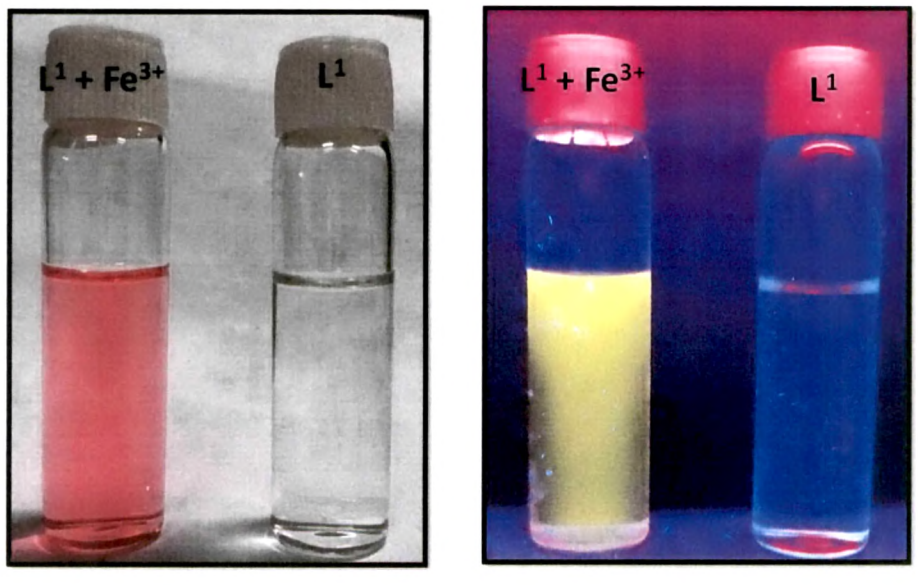

Figure 3.33. Change in colour (Left) and fluorescence (right) of L1 in CH_3CN/H_2O solution (1:1, v/v) with Fe^{3+} ions and blank.

Considering the behaviours of the fluorescence and absorption spectra, the off–on response of L^1 and L^2 may be explained by the spirocycle open–close mechanism. The free probe L^1 or L^2 is in the spirocyclic form, which is non-fluorescent, whereas coordination of Fe^{3+} leads to spirocycle opening, resulting in the appearance of visible absorption and fluorescence. The visible change in color can be used for the "naked-eye" detection of Fe^{3+} ions in an acetonitrile-aqueous environment (*see* Figure 3.33). Compounds L^1 and L^2 both show similar type of selectivity towards metal ions. On increasing the electron density over the phenyl ring attached to the nitrogen atom of pyrazolone ring in compound L^2, no changes are observed in the selectivity of compound L^2.

3.4. Conclusions

In summary, two new pyrazolone-rhodamine based signalling systems were designed and synthesized for the selective recognition of Fe^{3+} ions. The pyrazolone molecule was used as a recognition moiety and rhodamine-6G was used as a signalling moiety. The excellent colorimetric and fluorescent response to Fe^{3+} in CH_3CN/H_2O (1:1, v/v) can be detected even by the naked eye, which provides a facile method for the visual detection of Fe^{3+}. Complexation of the Fe^{3+} ion opens the spirolactum ring of rhodamine moieties to produce specific color change as well as fluorescence enhancement.

3.5. References

[1] A. W. Czarnik, *Chem. Biol.*, **1995**, *2*, 423-428.

[2] A. P. de Silva, H. Q. N. Gunaratne, T. Gunnlaugsson, A. J. M. Huxley, C. P. McCoy, J. T. Rademacher, T. E. Rice, *Chem. Rev.*, **1997**, *97*, 1515-1566.

[3] R. Martínez-Máñez, F. Sancenón, *Chem. Rev.*, **2003**, *103*, 4419-4476.

[4] J. S. Kim, D. T. Quang, *Chem. Rev.*, **2007**, *107*, 3780-3799.

[5] E. M. Nolan, S. J. Lippard, *Chem. Rev.*, **2008**, *108*, 3443-3480.

[6] R. N. Dsouza, U. Pischel, W. M. Nau, *Chem. Rev.*, **2011**, *111*, 7941–7980.

[7] A. Bencini, V. Lippolis, *Coord. Chem. Rev.*, **2012**, *256*, 149-169.

[8] K. Kaur, R. Saini, A. Kumar, V. Luxami, N. Kaur, P. Singh, S. Kumar, *Coord. Chem. Rev.*, **2012**, *256*, 1992-2028.

[9] M. Leermarkers, W. Baeyens, P. Quevauviller, M. Harvat, *Trends Anal. Chem.*, **2005**, *24*, 383-393.

[10] O. T. Butler, J. M. Cook, C. F. Harrington, S. J. Hill, J. Rieuwerts, D. J. Miles, *Anal. At. Spectrom.*, **2006**, *21*, 217-243.

[11] Y. Li, C. Chen, B. Li, J. Sun, J. Wang, Y. Gao, Y. Zhao, Z. Chai, *J. Anal. At. Spectrom.*, **2006**, *21*, 94-96.

[12] X. Chen, X. Tian, I. Shin, J. Yoon, *Chem. Soc. Rev.*, **2011**, *40*, 4783-4804.

[13] A. W. Czarnik, *Fluorescent chemosensors for ion and molecule recognition*, ACS Symp. Ser. 538, American Chemical Society, Washington, DC, **1993**.

[14] B. Valeur, I. Leray, *Coord. Chem. Rev.*, **2000**, *205*, 3-40.

[15] J. R. Lakowicz, *Principles of Fluorescence Spectroscopy,* Springer science, Singapore, **2006**.

[16] R. M. Duke, E. B. Veale, E. M. Pfeffer, P. E. Kruger, T. Gunnlaugsson, *Chem. Soc. Rev.*, **2010**, *39*, 3936-3953.

[17] M. Beija, C. A. M. Afonso, J. M. G. Martinho, *Chem. Soc. Rev.*, **2009**, *38*, 2410-2433.

[18] B. Valeur, *Molecular Fluorescence: Principles and Applications*, Wiley-VCH Verlag GmbH, **2001**.

[19] A. P. de Silva, S. A. de Silva, *J. Chem. Soc. Chem. Commun.*, **1986**, 1709-1710.

[20] A. P. de Silva, H. Q. N. Gunaratne, T. Gunnlaugsson, *Chem. Commun.*, **1996**, 1967-1968.

[21] G. De Santis, L. Fabbrizzi, M. Lichelli, C. Mangano, D. Sacchi, N. Sardone, *Inorg. Chim. Acta*, **1997**, *257*, 69-76.

[22] K. Golchini, M. Mackovic-Basic, S. A. Gharib, D. Masilamani, M. E. Lucas, I. Kurtz, *Am. J. Physiol.*, **1990**, *258*, F438-F443.

[23] L. Fabbrizzi, M. Lichelli, P. Pallavicini, A. Taglietti, *Inorg. Chem.*, **1996**, *35*, 1733-1736.

[24] L. Fabbrizzi, M. Lichelli, P. Pallavicini, D. Sacchi, A. Taglietti, *Analyst*, **1996**, *121*, 1763-1767.

[25] R. Bergonzi, L. Fabbrizzi, M. Lichelli, C. Mangano, *Coord. Chem. Rev.*, **1998**, *170*, 31-46.

[26] H. C. Cheung, Principles, in: J. R. Lakowicz (Ed.), Topics in Fluorescence Spectroscopy, vol. 2, Kluwer Academic Publishers, New York, **2002**, Chapter 3.

[27] K. E. Sapsford, L. Berti, I. L. Medintz, *Angew. Chem. Int. Ed.*, **2006**, *45*, 4562-4588.

[28] J. R. Albani, *Principles and Applications of Fluorescence Spectroscopy*, Blackwell Science, Oxford, UK, **2007**, Chapter 14.

[29] M. Suresh, S. Mishra, , S. K. Mishra, E. Suresh, A. K. Mandal, A. Shrivastav, A. Das, *Org. Lett.*, **2009**, *11*, 2740-2743.

[30] Z. Zhou, M. Yu, H. Yang, K. Huang, F. Li, T. Yi, C. Huang, *Chem. Commun.*, **2008**, 3387–3389.

[31] B. Valeur, J. Bourson, J. Pouget, in: A.W. Czarnik (*eds.*), *Fluorescent Chemosensors for Ion and Molecule Recognition*, ACS Symposium Series 538, American Chemical Society, Washington, DC, **1993**, p. 25.

[32] W. Rettig, R. Lapouyade, *Probe design and chemical sensing*, in: J. R. Lakowicz (*ed.*), Topics in Fluorescence Spectroscopy, vol. 4, Plenum, New York, **1994**, p. 109.

[33] B. Valeur, F. Badaoui, E. Bardez, J. Bourson, P. Boutin, A. Chatelain, I. Devol, B. Larrey, J. P. Lefèvre, A. Soulet, in: J.-P. Desvergne, A.W. Czarnik (*eds.*), *Chemosensors of Ion and Molecule Recognition*, NATO ASI Series, Kluwer, Dordrecht, **1997**, p. 195.

[34] J. Bourson, B. Valeur, *J. Phys. Chem.*, **1989**, *93*, 3871-3876.

[35] S. Fery-Forgues, M. -T. Le Bris, J. -P. Guetté, B. Valeur, *J. Chem. Soc. Chem. Commun.*, **1988**, *5*, 384-385.

[36] S. Fery-Forgues, M.-T. Le Bris, J.-P. Guetté, B. Valeur, *J. Phys. Chem.*, **1988**, *92*, 6233-6237.

[37] S. Fery-Forgues, J. Bourson, L. Dallery, B. Valeur, *New J. Chem.*, **1990**, *14*, 617-623.

[38] G. A. Smith, T. R. Hesketh, J. C. Metcalfe, *Biochem. J.*, **1988**, *250*, 227-232.

[39] S. J. Lee, J. H. Jung, J. Seo, II. Yoon, K-M. Park, L. F. Lindoy, S. S. Lee, *Org. Lett.*, **2006**, *8*, 1641.

[40] Z. Xu, Y. Xiao, X. Qian, J. Cui, D. Cui, *Org. Lett.*, **2005**, *7*, 889.

[41] X. Chen, T. Pradhan, F. Wang, J. S. Kim, J. Yoon, *Chem. Rev.*, **2012**, *112*, 1910-1956.

[42] E. Noelting, K. Dziewonsky, *Ber. Dtsch. Chem. Ges.*, **1905**, *38*, 3516-3527.

[43] (a) R. P. Haugland, *Handbook of Fluorescent Probes and Research Chemicals*, 9th Ed.; *Molecular Probes*: Eugene, OR, 2002; (b) F. Amat-

Guerri, A. Costela, J. M. Figuera, F. Florido, R. Sastre, *Chem. Phys. Lett.*, **1993**, *209*, 352-356.

[44] V. Dujols, F. Ford, A. W. Czarnik, *J. Am. Chem. Soc.*, **1997**, *119*, 7386-7387.

[45] Y. Xiang, Z. Li, X. Chen, A. Tong, *Talanta*, **2008**, *74*, 1148-1153.

[46] J. F. Zhang, Y. Zhou, J. Yoon, Y. Kim, S. J. Kim, J. S. Kim, *Org. Lett.*, **2010**, *12*, 3852-3855.

[47] P. Xi, J. Dou, L. Huang, M. Xu, F. Chen, Y. Wu, D. Bai, W. Li, Z. Zeng, *Sens. Actuators B*, **2010**, *B148*, 337-341.

[48] S. H. Mashraqui, T. Khan, S. Sundaram, R. Betkar, M. Chandiramani, *Chem. Lett.*, **2009**, *38*, 730-731.

[49] M. Suresh, A. Shrivastav, S. Mishra, E. Suresh, A. Das, *Org. Lett.* **2008**, *10*, 3013-3061.

[50] J. Mao, L. Wang, W. Dou, X. Tang, Y. Yan, W. Liu, *Org. Lett.*, **2007**, *9*, 4567-4570.

[51] M. H. Lee, T. V. Giap, S. H. Kim, Y. H. Lee, C. Kang, J. S. Kim, *Chem. Commun.*, **2010**, *46*, 1407-1409.

[52] K.-S. Moon, Y.-K. Yang, S.-H. Ji, J.-S. Tae, *Tetrahedron Lett.*, **2010**, *51*, 3290-3293.

[53] L. Yuan, W. Lin, Y. Yang, *Chem. Commun.*, **2011**, *47*, 6275-6277.

[54] W. Huang, D. Wu, D. Guo, X. Zhu, C. He, Q. Meng, C. Duan, *Dalton Trans.*, **2009**, 2081-2084.

[55] H. Kim, S. Lee, J. Lee, J. Tae, *Org. Lett.*, **2010**, *12*, 5342-5345.

[56] (*a*) P. Aisen, M. Wessling-Resnick, E. A. Leibold, *Curr. Opin. Chem. Biol.*, **1999**, *3*, 200–206; (*b*) R. S. Eisenstein, *Annu. Rev. Nutr.*, **2000**, *20*, 627–662; (*c*) T. A. Rouault, *Nat. Chem. Biol.*, **2006**, *2*, 406–414.

[57] (*a*) H. Weizman, O. Ardon, B. Mester, J. Libman, O. Dwir, Y. Hadar, Y. Chen, A. Shanzer, *J. Am. Chem. Soc.*, **1996**, *118*, 12386; (*b*) R. Nudelman, O. Ardon, Y. Hadar, Y. Chen, J. Libman, A. J. Shanzer, *Med. Chem.*, **1998**, *41*, 1671; (*c*) L. Ma, W. Luo, P. J. Quinn, Z. Liu, R. C. Hider, *J. Med. Chem.*, **2004**, *47*, 6349-6362; (*d*) V. P. Boricha, S. Patra, S. Parihar, Y. S. Chouhan, P. Paul, Polyhedron, **2012**, 43, 104-113

[58] (*a*) Z. -Q. Hu, X. -M. Wang, Y. -C. Feng, L. Ding, M. Li, C. –S. Lin, *Chem. Commun.*, **2011**, *47*, 1622-1624; (*b*) B. Bag, B. Biswal, *Org. Biomol. Chem.*, **2012**, *10*, 2733-2738; (*c*) Z. Aydin, Y. Wei, M. Guo, *Inorg. Chem. Commun.*,

2012, *20*, 93-96; (*d*) Z. Yang, M. She, B. Yin, J. Cui, Y. Zhang, W. Sun, J. Li, Z. Shi, *J. Org. Chem.*, **2012**, *77*, 1143-1147.

[59] (*a*) J. Xu, K. N. Raymond, *Angew. Chem. Int. Ed.*, **2000**, *39*, 2745-2747; (*b*) J. S. Casas, M. S. García-Tasende, A. Sánchez, J. Sordo, A. Touceda, *Coord. Chem. Rev.*, **2007**, *251*, 1561–1589; (*c*) K. Hellmuth, S. Grosskopf, C. T. Lum, M. Würtele, N. Röder, J. P. Kries, M. Rosario, J. Rademann, W. Birchmeier, *Proc. Natl. Acad. Sci. USA*, **2008**, *105*, 7275-7280; (*d*) R. N. Jadeja, S. Parihar, K. Vyas, V. K Gupta, *J. Mol. Struct.*, **2012**, *1013*, 86–94; (*e*) S. Parihar, S. Pathan, R. N. Jadeja, A. Patel, V. K. Gupta, *Inorg. Chem.*, **2012**, *51*, 1152-1161.

[60] (*a*) H. -J Park, K. Lee, S. -J. Park, B. Ahn, J. –C. Lee, H. Y. Cho, K. –I. Lee, *Bioorg. Med. Chem. Lett.*, **2005**, *15*, 3307–3312; (*b*) G. Ouyang, X. J. Cai, Z. Chen, B. A. Song, P. S. Bhadury, S. Yang, L. H. Jin, W. Xue, D. Y. Hu, S. Zeng, *J. Agric. Food Chem.*, **2008**, *56*, 10160–10167; (*c*) V. Marković, S. Erić, Z. D. Juranić, T. Stanojković, L. Joksović, B. Ranković, M. Kosanić, M. D. Joksović, *Bioorg. Chem.*, **2011**, *39*, 18-27.

[61] (*a*) H. G. Li, Z. Y. Yang, D. D. Qin, *Inorg. Chem. Commun.*, **2009**, *12*, 494-497; (*b*) T. Li, Z. Yang, Y. Li, Z. Liu, G. Qi, B. Wang, *Dyes Pigm.*, **2011**, *88*, 103-108; (*c*) Y. Lei, Y. Su, J. Huo, *J. Luminesc.*, **2011**, *131*, 2521-2527; (*d*) H. H. Zhang, W. Dou, W. S. Liu, X. L. Tang, W. W. Qin, *Eur. J. Inorg. Chem.*, **2011**, *2011*, 748–753.

[62] G. He, D. Guo, C. He, X. Zhang, X. Zhao, C. Duan, *Angew. Chem. Int. Ed.*, **2009**, *48*, 6132-6135.

[63] (*a*) Y. Xiang, A. Tong, *Org. Lett.*, **2006**, *8*, 1549-1552; (*b*) Z. Aydin, Y. Wei, M. Guo, Inorg. *Chem. Commun.*, **2012**, *20*, 93-96; (*c*) N. R. Chereddy, S. Thennarasu, A. B. Mandal, *Dalton Trans.*, **2012**, *41*, 11753–11759.

[64] X. Zhang, Y. Shiraishi, T. Hirai, *Tetrahedron Lett.*, **2007**, *48*, 5455-5459.

[65] (*a*) K. A. Connors, *Binding Constants, the Measurement of Molecular Complex Stability*, John Wiley & Sons: New York, **1987**, pp 24-28; (*b*) P. Das, A. Ghosh, A. Das, *Inorg. Chem.*, **2010**, *49*, 6909-6916 and references cited therein.

[66] S. Huang, P. Du, C. Min, Y. Liao, H. Sun, Y. Jiang, *J. Fluoresc.*, **2013**, *23*, 621-627.

Research article

LUMINESCENCE
The Journal of Biological and Chemical Luminescence

Received: 10 December 2013, Revised: 9 April 2014, Accepted: 2 May 2014 Published online in Wiley Online Library

(wileyonlinelibrary.com) DOI 10.1002/bio.2709

Pyrazolone as a recognition site: Rhodamine 6G-based fluorescent probe for the selective recognition of Fe^{3+} in acetonitrile–aqueous solution

Sanjay Parihar,[a] Vinod P. Boricha[b] and R. N. Jadeja[a]*

ABSTRACT: Two novel Rhodamine–pyrazolone-based colorimetric off–on fluorescent chemosensors for Fe^{3+} ions were designed and synthesized using pyrazolone as the recognition moiety and Rhodamine 6G as the signalling moiety. The photophysical properties and Fe^{3+}-binding properties of sensors L^1 and L^2 in acetonitrile–aqueous solution were also investigated. Both sensors successfully exhibit a remarkably 'turn-on' response, toward Fe^{3+}, which was attributed to 1: 2 complex formation between Fe^{3+} and L^1/L^2. The fluorescent and colorimetric response to Fe^{3+} can be detected by the naked eye, which provides a facile method for the visual detection of Fe^{3+}. Copyright © 2014 John Wiley & Sons, Ltd.

Additional supporting information may be found in the online version of this article at the publisher's web site.

Keywords: Rhodamine; pyrazolone; fluorescence; Job plot; ion recognition

Introduction

The design and synthesis of new chemosensors for selective detection of heavy and transition metal (HTM) cations are important subjects in the field of supramolecular chemistry due to their significance in chemical, biological and environmental assays (1–5). Fluorescent sensors are of particular interest because they allow non-destructive and quick detection using a simple fluorescent enhancement (turn-on) or quenching (turn-off) response (6–9). Fluorescent chemosensors combine two fundamental functional units: a fluorophore and an ionophore. The ionophore can selectively bind the substrate, and the fluorophore is attached in the vicinity of the binding site for signal detection and transduction. A large number of fluorescent sensors have been designed to detect different types of heavy toxic metal ions. In the fluorescent detection of ions, fluorescence enhancement ('turn-on') is preferable to fluorescence quenching ('turn-off'), because the former lessens the chance of false-positive data from other fluorescent quenchers existing in samples (10).

Recently, Rhodamine amide derivatives have been widely used as fluorescent probes for the detection of various ions (9,11–15). The Rhodamine framework is an ideal mode for the construction of fluorescent chemosensors, owing to their excellent photophysical properties, such as long absorption and emission wavelengths, large absorption coefficient, and high fluorescence quantum yield (16). The cation-sensing mechanism of these probes is based on structural changes between the spirocyclic and open-cycle forms (11,12). Without cations, the probes exist in a spirocyclic form, which is less or non-fluorescent. The addition of metal cations leads to opening of the spirocycle, resulting in the appearance of pink and orange fluorescence. The additional advantage of such a Rhodamine-based sensing system is that the ring-opening process is accompanied by a vivid change from colourless to pink, thus enabling the metal detection with the naked eye.

The selective detection of biologically important metal ions has become tremendously important because metal ions are involved in a variety of fundamental biological processes in organisms. Iron is one of the most important metals in biological systems and plays a key role at the cellular level in many biochemical processes. Specifically, ferric ions (Fe^{3+}) are widely retained in many proteins and enzymes either for structural purposes or as part of a catalytic site (17–19). Moreover, the ferric ion is well-known as a fluorescence quencher due to its paramagnetic nature, and most reported Fe^{3+} receptors, such as analogues of ferrichromes or siderophores, undergo fluorescence quenching when bound with Fe^{3+} (20–22), although it is generally believed that probes with a fluorescence enhancement signal on interacting with analytes are much more efficient. Therefore, the development of new fluorescent indicators for the accurate and specific detection of Fe^{3+}, especially indicators that exhibit selective Fe^{3+}-amplified emission, remains a challenge. Recently, a few sensors have been described to exhibit a turn-on response to Fe^{3+} ions (23–26).

* Correspondence to: R. N. Jadeja, Department of Chemistry, Faculty of Science, The M. S. University of Baroda, Vadodara 390002, India. E-mail: rajendra_jadeja@yahoo.com

[a] Department of Chemistry, The M. S. University of Baroda, Vadodara 390002, India

[b] Analytical Science Division, Central Salt and Marine Chemicals Research Institute (Constituents of CSIR, New Delhi), G. B. Marg, Bhavnagar 364002, India